International Journal of Greenhouse Gas Control 123 (2023) 103838

Contents lists available at ScienceDirect

International Journal of Greenhouse Gas Control

journal homepage: www.elsevier.com/locate/ijggc

Reservoir properties and reactivity of the Faroe Islands Basalt Group: Investigating the potential for CO_2 storage in the North Atlantic Igneous Province

Marija P. Rosenqvist [a,*], Max W.J. Meakins [b,1], Sverre Planke [c,d], John M. Millett [c,e], Hans Jørgen Kjøll [b], Martin J. Voigt [f,g], Bjørn Jamtveit [a]

[a] The Njord Centre, University of Oslo, Norway
[b] Department of Geosciences, University of Oslo, Norway
[c] Volcanic Basin Energy Research (VBER), Norway
[d] Centre for Earth Evolution and Dynamics (CEED), University of Oslo, Norway
[e] Department of Geology and Geophysics, University of Aberdeen, United Kingdom
[f] Institute of Earth Science, University of Iceland, Iceland
[g] Carbfix, Iceland

ARTICLE INFO

Keywords:
CO_2 sequestration
Mineral storage
Mineral carbonation
Basalt carbonation
Faroe Islands Basalt Group
North Atlantic Igneous Province

ABSTRACT

Offshore injection of CO_2 into volcanic sequences of the North Atlantic Igneous Province may present a large-scale, permanent storage option through carbonate mineralization. To investigate this potential, onshore studies of reservoir properties and reactivity of the subaerially erupted Faroe Islands Basalt Group have been conducted. Outcrop and borehole samples reveal that the lava flow crusts commonly contain vesicles that have been filled with secondary minerals due to hydrothermal fluid circulation, however, unmineralized and highly porous layers do occur. Bulk density measurements, micro-computed tomography (μ-CT) image analysis, and microscope studies of samples from onshore boreholes give present-day porosities ranging from 0.5% to 36.2% in the volcanic sequences. The unmineralized brecciated lava flow crusts contain the largest estimated porosity and simulated absolute permeability (reaching up to 10^{-12} m^2). μ-CT studies of the mineralized, brecciated flow crusts indicate initial porosities reaching up to 45%, before clogging. Kinetic experiments of rock dissolution show that the reactivity of the basalt and volcaniclastic sediments depends on the alteration state with more altered basalt being less reactive. However, the presence of reactive, high porosity, and high permeability flow crusts prior to clogging indicate the existence of promising and very large CO_2 reservoirs in less altered offshore sequences.

1. Introduction

Climate change will cause significant damage and cost to society unless the anthropogenic greenhouse gas emissions are substantially reduced in the next ca. 30 years (IPCC, 2021). To reach the goal of the Paris Agreement (UN, 2015) of limiting global warming to 1.5 °C by 2050, removing carbon from the atmosphere has to be part of the solution (IPCC, 2018). Safe storage of captured CO_2 will, therefore, play a vital role in the future of industry (IEA, 2021; IPCC, 2018). Several studies have shown the feasibility of storing CO_2 in mafic rocks such as basalt (e.g., Matter et al., 2011; McGrail et al., 2011). CO_2 reacts with the divalent cations, e.g., Ca^{2+}, Mg^{2+}, and Fe^{2+}, dissolved from the mafic rocks, leading to the formation of various carbonate minerals, and storing the carbon for geological timescales (McGrail et al., 2006). Carbonate minerals such as calcite ($CaCO_3$), dolomite ($Ca_{0.5}Mg_{0.5}CO_3$), magnesite ($MgCO_3$), siderite ($FeCO_3$), and ankerite ($Ca(Fe^{2+}, Mg)(CO_3)_2$) may form (Benson et al., 2005). The reactions are described by, e.g., Gislason et al. (2014) and are as follows:

1 Dissolution of CO_2 (gas) in water and freeing of H^+-ions:

Abbreviations: FIBG, Faroe Islands Basalt Group; NAIP, North Atlantic Igneous Province; CRBG, Columbia River Basalt Group.

* Corresponding author.
E-mail address: m.p.rosenqvist@mn.uio.no (M.P. Rosenqvist).

[1] Rosenqvist and Meakins co-lead this study.

https://doi.org/10.1016/j.ijggc.2023.103838
Received 6 July 2022; Received in revised form 28 November 2022; Accepted 13 January 2023
Available online 25 January 2023

$$CO_2(g) + H_2O\ (l) \rightleftharpoons H_2CO_3\ (aq) \rightleftharpoons HCO_3^- + H^+$$

2 Dissolution of basaltic glass and primary minerals:

$$Basaltic\ glass + xH^+ \rightarrow Mg^{2+} + Ca^{2+} + Fe^{2+} + \ldots$$

$$Mg_2SiO_4(forsterite) + 4H^+ \rightarrow 2Mg^{2+} + 2H_2O + SiO_2(aq)$$

$$MgCaSi_2O_5(diopside) + 4H^+ \rightarrow Mg^{2+} + Ca^{2+} + 2H_2O + 2SiO_2(aq)$$

$$CaAl_2Si_2O_8(Ca-plagioclase) + 8H^+ \rightarrow Ca^{2+} + 2Al^{3+} + 2SiO_2(aq) + 4H_2O$$

3 Precipitation of carbonate minerals:

$$(Mg,\ Ca,\ Fe)^{2+} + CO_2 + H_2O \rightarrow (Ca, Mg, Fe)CO_3(carbonates) + 2H^+$$

Other minerals that may form are Al- and Fe-hydroxides, chalcedony, zeolites, and smectite (Snæbjörnsdóttir et al., 2018). Field experiments indicate near complete mineralization of CO_2 injected into basalt formations within two years if the CO_2 is injected into the reservoir in water-dissolved form (Matter et al., 2016). In comparison, it generally takes several thousands of years for significant amounts of CO_2 to mineralize in a more conventional siliciclastic reservoir or if pure CO_2 is injected (Benson et al., 2005). Basalt also provides large reservoir volumes for carbon storage, present in Large Igneous Provinces (LIPs) and mid-oceanic ridges around the world (Gíslason and Oelkers, 2014; McGrail et al., 2006).

Pilot studies in Iceland (Carbfix and Carbfix2) and in the US (Wallula) have shown the feasibility of storing CO_2 in onshore basalt reservoirs by mineral trapping (Matter et al., 2011; McGrail et al., 2011). The Wallula pilot project started injecting CO_2 as a supercritical fluid into the Columbia River Flood Basalt in 2013 (McGrail et al., 2017). Results showed that some of the CO_2 mineralized already within 24 months after emplacement. Free-phase CO_2 was still present at the top of the reservoir and held in place by an impermeable flow core caprock (McGrail et al., 2017). The Carbfix pilot project in Iceland started its pilot injection and

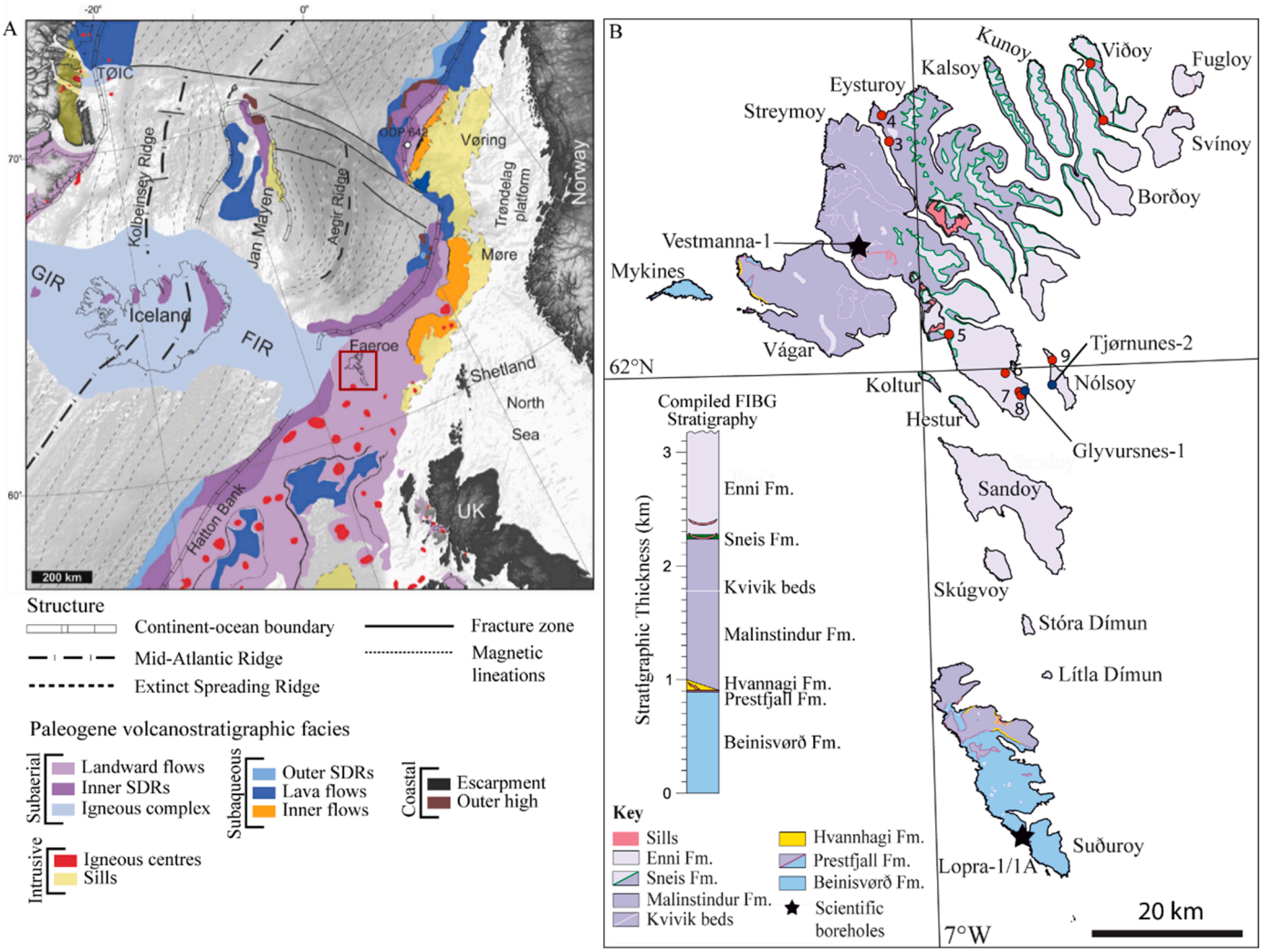

Fig. 1. Overview of the study area. **A)** Map showing the extent of the North Atlantic Igneous Province, with the location of the Faroe Islands marked. The different volcanic facies are indicated (modified from Abdelmalak et al., 2017; Planke et al., 2020). **B)** Geological map and stratigraphic column for the Faroe Islands with field (red dots) and borehole locations (blue dots) indicated (modified from Passey and Jolley, 2009). Further details about localities 1–9 can be found in the Supplements.

monitoring in 2012, and industrial-scale operation began in 2014 (Gíslason et al., 2018). In all Carbfix injections, CO_2 is dissolved in water before or during injection (Gunnarsson et al., 2018; Sigfusson et al., 2015). Dissolving the CO_2 in water removes the need for a caprock as the gas is no longer buoyant, as well as dramatically reducing the time needed to achieve CO_2 mineral trapping. Among others, the project is currently injecting around 12,000 tons of CO_2 per year into an onshore basalt reservoir at about 800 m depth and a temperature of around 250 °C (Snæbjörnsdóttir et al., 2020). Results show that ca. 65% of the CO_2 is mineralized as carbonates within two months after injection, and there is no observed decrease in reservoir permeability or mineralization rates since injection started in 2014 (Clark et al., 2020; Gunnarsson et al., 2018).

The availability of the relatively young onshore basalt sequences to react and store CO_2 on a smaller scale is well documented through the two aforementioned projects. However, in the future, offshore storage in volcanic margin basalt sequences is likely to hold the largest storage potential (Goldberg et al., 2008; Snæbjörnsdóttir et al., 2014), given that the potential of rapid mineralization in the seawater-CO_2-basalt has been confirmed experimentally (Voigt et al., 2021). The North Atlantic Igneous Province (NAIP; Fig. 1A) stretches around 2000 km between eastern Canada to the British Isles and may provide several potential offshore storage sites for CO_2 (Planke et al., 2020; Saunders et al., 1997). There is a need for better constraints on the potential for CO_2 storage in the offshore sequences of the NAIP. In this study, we characterize the reservoir properties and reactivity of the effusive basalt sequences cropping out on the Faroe Islands, NE Atlantic Ocean (Fig. 1A). The Faroe Islands Basalt Group (FIBG) offer spectacular outcrop exposures of an uplifted part of the NAIP that forms a representative analogue for large regions of the subsurface along the UK, Faroese, Norwegian, and Greenland margins. By the combination of detailed petrophysical and geochemical descriptions of the rocks in the upper two formations of the FIBG, namely the Malinstindur and Enni formations, we identify potential reservoir and caprock lithologies in volcanic sequences of the North Atlantic Igneous Province, relevant for the appraisal of potential volcanic CO_2 reservoirs.

1.1. Geological framework

The exposed stratigraphy on the Faroe Islands is a part of the Faroe Islands Basalt Group (FIBG; Passey and Jolley, 2009). The stratigraphic thickness of the FIBG is $>$ 6.6 km, where ca. 3.2 km is exposed on the Faroe Islands (Chalmers and Waagstein, 2006; Ellis et al., 2002). Seven different formations are recognized of which six are exposed on the islands and the deepest, the Lopra Formation, is only accessed through the deep Lopra 1/1A borehole; Fig. 1) (Passey and Jolley, 2009). The Malinstindur and Enni formations are the uppermost exposed basalt units and were chosen as the primary targets for the sampling and reservoir characterization in this study. These formations are likely least affected by secondary mineralization, shown to increase with burial depth, and therefore more likely to contain sections with good reservoir properties (open porosity; Neuhoff et al., 1999; Walton and Schiffman, 2003). Two geometric lava flow types are generally recognized in the Malinstindur and Enni formations: simple (or tabular) lava flows and compound-braided lava flows (Walker, 1972). Compound lava flows can be divided into several individual flow lobes, while simple flows consist of an individually inflated flow lobe (Walker, 1972).

The Malinstidur Formation has a gross stratigraphic thickness of 1050 – 1350 m on the Faroe Islands and consists of compound-braided lava flows with an average thickness of 20 m (Passey and Bell, 2007; Rasmussen and Noe-Nygaard, 1970; Waagstein, 1988). The Enni Formation is the uppermost exposed unit on the Faroe Islands, where it has a stratigraphic thickness of at least ca. 900 m (Passey and Jolley, 2009). It is estimated from zeolite studies that about 1 km of overburden has been eroded from above the exposed Enni Formation (Jørgensen, 2006; Waagstein et al., 2002b). The formation comprises both simple and compound-braided lava flows, where the simple flows have an average thickness of ca. 15 m, while the compound layers can be several tens of meters thick (Noe-Nygaard and Rasmussen, 1968; Passey and Jolley, 2009; Rasmussen and Noe-Nygaard, 1970). Lava flow lobes are generally seen to have a classic internal architecture consisting of an upper and lower crust (either brecciated or vesicular) with a massive flow core between (Waagstein, 1998). The flow crusts of basalt lava flows are likely to present the best prospects for finding high porosities and high permeabilities as these are often highly vesicular (Couves, 2015; Eidesgaard, 2021; Planke et al., 2020).

The Sneis Formation ($<$ 30 m thick) rests between the Malinstindur and Enni formations and consists of a volcaniclastic sandstone-conglomerate pairing (Passey and Jolley, 2009). Thin, volcaniclastic interbeds, or red beds can also be found between the flows in both the Malinstindur and Enni formations (Passey and Jolley, 2009). Several stages of deformation during and after the emplacement of the FIBG have led to the formation of mainly normal and strike-slip faults, fractures, and intrusions cutting through the layers (e.g., Walker et al., 2011a). The FIBG is generally seen to dip towards the SE except on Suðuroy (Fig. 1), where it dips towards the NE and the stratigraphically highest units can be found on the NE and SE islands (Waagstein, 1988).

2. Data and methods

The fieldwork for this study was conducted on the Faroe Islands in June 2020. In addition, borehole data consisting of both wireline logs and cores were accessed. Samples were collected in the field and from the cores and analysed in the lab by optical microscopy, Scanning Electron Microscope (SEM), 3-D X-ray μ-CT (computed tomography) image analysis, and bulk density measurements. Mineralogical and geochemical analyses of five field samples were combined with kinetic experiments to study the reactivity of the rocks. A full and detailed description of the data and methodology in this study can be found in the online supplementary material.

Nine key localities on the Faroe Islands were chosen for outcrop studies and sampling (Fig. 1B). The visited localities cover the upper ca. 500 m of the Malinstindur Formation and the lower ca. 350 m of the Enni Formation and provided a geological context for the boreholes. Outcrop observations were documented using pictures, field notes, sketches, and samples. Eight samples were collected in the field where five were used for the reactivity experiments and three were used for μ-CT image analysis. Samples were also collected from two onshore boreholes (Glyvursnes-1 and Tjørnunes-2; Fig. 1B). Data from the Glyvusnes-1 borehole consisted of core photographs, wireline log data, a lithological log, and 40 samples, while the data from the Tjørnunes-2 borehole consisted of core photos, lithological logs, and 8 samples. Flows 3, 4, and 17 in the Glyvursnes-1 borehole and Flow FVII (part of the FVII or Tjørnunes Flow; Jolley and Passey, 2012) in the Tjørnunes-2 were chosen for the case studies of porosity and permeability and were subject to close sampling and lithological logging (Figs. 2B and C). The lava flows in the Glyvursnes-1 borehole have previously been named F1-F37 according to Waagstein (1988) while the lava flows in the Tjørnunes-2 borehole and the ones sampled for the kinetic experiment samples are named FI-FXVII according to Jolley and Passey (2012).

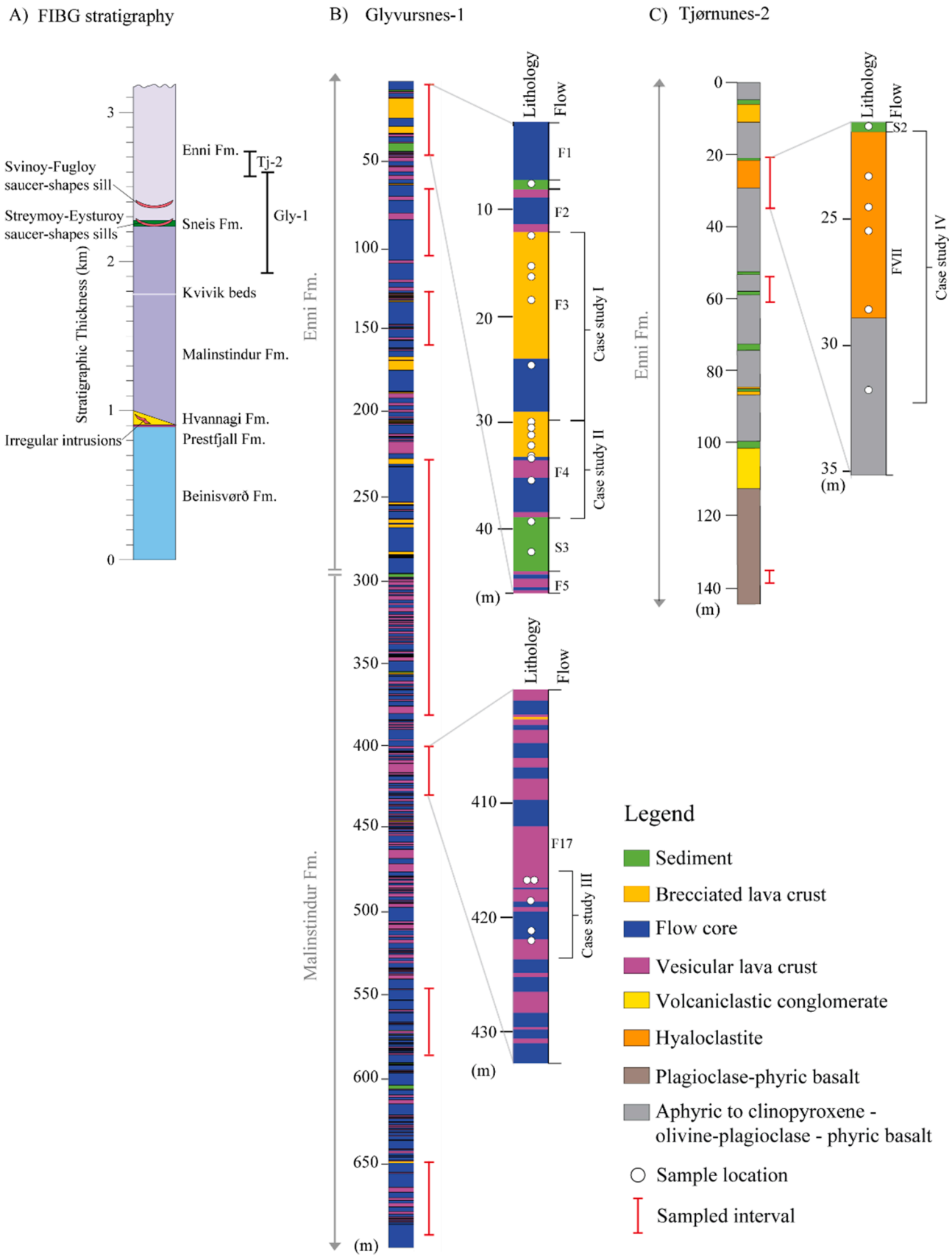

Fig. 2. Overview of boreholes used in this study. **A)** Stratigraphic locations of the Tjørnunes-2 (Tj-2) and Glyvursnes-1 (Glyv-1) boreholes (modified from Passey and Jolley, 2009). **B)** Lithological log of the Glyvursns-1 borehole with sample locations indicated (modified from Waagstein, 2002a). **C)** Lithological log of the Tjørnunes-2 borehole with sample locations indicated (modified from Jolley and Passey, 2012). Case study intervals are marked.

2.1. Porosity from the density log

The wireline log from the Glyvursnes-1 borehole contains optical televiewer, three-arm calliper, formation density, focused electric, full wave-form/compensated sonic, natural gamma spectroscopy, and temperature/conductivity data. The neutron-porosity log could not be used as a direct indicator of porosity without mineralogical calibration as the response of the neutron tool is highly sensitive to hydrous minerals such as clays and zeolites which are numerous in the Faroe Islands basalts (Broglia and Ellis, 1990; Jørgensen, 1984). Therefore, the density log from the Glyvursnes-1 borehole was used to calculate two end-member porosity logs based on grain density estimates from the density log (2.85 g/cm^3 for fresh basalt) and from Ólavsdóttir et al. (2015) (2.61 g/cm^3 for volcaniclastic interbeds and altered basalts). Calculations were performed using the method described by, e.g., Schlumberger (1987).

2.2. Laboratory analyses

Polished, uncovered, and epoxy-impregnated thin sections were produced for all the samples and studied using optical microscopy to identify mineralogy, textures, and structural features. Selected thin sections were analysed using SEM and used to study the mineralogy, petrography, and porosity of the samples (Reed, 2005). Energy dispersive spectroscopy (EDS) was used to identify the minerals and obtain elemental distribution maps (Reed, 2005).

Eight flow crust samples from the Glyvursnes-1 and two breccia samples from the Tjørnunes-2 core were scanned for micro-computed tomography using the *Nikon Metrology XT H 225 ST* instrument at the Natural History Museum, at the University of Oslo. The scans were used to look at the pore volume (porosity), largest connected pore space, and pore diameters in the sample volumes. The secondary minerals and the open porosity were used together to study the primary porosity of the samples. In addition, core plugs from three samples, collected in the field, were scanned at the European Synchrotron Radiation Facility (ESRF) in Grenoble, France, to obtain higher resolution. Processing and analysis of the scans generally follow the method of Callow et al. (2018) with adjustments to this sample set. Three samples were then chosen for fluid flow simulations to obtain permeability estimates. The simulation uses Stokes equations and later Darcy's law to determine the absolute permeability of the sample volume (Avizo, 2016; Bernard et al., 2005).

The ImageJ software (Ferreira and Radband, 2012) was used to study the microporosity of the basalt groundmass and volcaniclastic sediments. The porosity was determined from thin sections of selected flow cores and sedimentary beds in the two boreholes, by applying a thresholding function on three different Backscatter Electron (BSE) images in each thin section. In addition, five flow crust samples from the Glyvursnes-1 borehole were used to estimate the porosity from the density using the previous matrix density estimate of 2.61 g/cm^3 (see Section 2.2). This was done to estimate the total porosity of the flow crust samples, including the porosity below CT resolution.

Kinetic experiments were performed to constrain the dissolution rates of the rocks. Representative volumes of five samples were collected for analysis of whole-rock chemistry, using Inductively Coupled Plasma Mass Spectrometry (ICP-MS). Powdered sample materials with a grain size range of 45–125 μm were prepared for the kinetic experiments, following the methods of Stockmann et al. (2011) and Gudbrandsson et al. (2011, 2014). The specific surface areas were quantified based on the Brunner-Emmett-Teller Theory (BET; Brunauer et al., 1938) using a Microtrac BELSORP MAX analyser. The kinetic experiments follow the general method of Gudbrandsson et al. (2014). In brief, a pH solution was pumped through a stirred reactor containing ca. 4 g of powdered sample at a rate of 2 g/min until steady-state outlet compositions were achieved. Periodic measurements of outlet solution pH, flow rate, and ion concentrations (Si, Na, K, Ca, Mg, and Fe) using Inductively Coupled Plasma Optical Emission Spectroscopy (ICP-OES) then allow calculation and interpretation of dissolution rates. The dissolution rates are reported as normalized to the BET specific surface areas to enable comparison to others experiments and to enable scaling to field scale data and models, as the reactive surface area of powdered rock is higher than for a field-scale injection scenario.

3. Results

3.1. Upper FIBG stratigraphy and flow architectures

3.1.1. Field observations

The results from the fieldwork show that the lower Enni Formation contains zones, up to ca. 50 m thick and more than 5 km long, of largely weathered lava flows interpreted as compound-braided lava flow packages (Fig. 3A). The compound-braided flow lobes extend for ca. 1 m – ca. 20 m and have a thickness typically between ca. 20 cm and ca. 2 m. Large tabular benches, interpreted as simple lava flows, stick out between the compound braided-flow packages (Fig. 3A). The simple flows extend for several hundred meters (up to several kilometres), with an estimated thickness between ca. 2 m – ca. 20 m (Fig. 3A). In addition, thin (generally <1 m thick), volcaniclastic "red beds" can be observed between lava flows. The upper Malinstindur Formation contains mainly compound-braided lava flows interbedded by thin (<1 m thick) volcaniclastic sediments (Fig. 3B).

The flow lobes at the studied localities were mainly observed to comprise 1) a thin vesicular base, often with pipe vesicles, 2) a massive flow core containing some subvertical fractures/veins and a few isolated vesicles/amygdales, and 3) a flow top, dense with vesicles/amygdales (Fig. 3C). The observed lava flow crusts are mostly vesicular confirming pahoehoe flow facies. In some examples, rubbly or brecciated upper flow crusts are identified indicating transitional rubbly pahoehoe to Aa lava flow facies, however, lower crusts were often harder to observe due to exposure making this distinction challenging. Smaller- and larger-scale intrusions, faults, joints, and fractures were also observed to cut through the studied formations throughout the islands (e.g., Locality 1; Fig 3A).

3.1.2. Glyvursnes-1 logs

In the Glyvursnes-1 borehole, the lava flows have a thickness ranging between ca. 0.5 m and 78 m. The upper lava flow crusts of the Enni Formation are between ca. 20 cm and 13 m thick, while the flow cores are between ca. 0.5 m and ca. 25 m. The thicknesses of the flow crusts in the Malinstindur Formation are between ca. 20 cm and 6 m, while the flow cores have thicknesses between ca. 0.5 m and ca. 14 m. The Φ_1 log, the porosity log for a matrix density of 2.85 g/cm^3, indicates a basalt flow crust porosity (assuming minor alteration) generally between ca. 5% and ca. 55%, and flow core porosities below ca. 10%. The Φ_2 log, for a matrix density of 2.61 g/cm^3, indicates a sediment porosity between ca. 5% and 35% in the Enni Formation and between ca. 5% and ca. 15% for the Sneis and Malinstindur formations. The log also plots a flow crust porosity (assuming the crusts are severely altered) up to ca. 45%. Negative values in the calculated porosity logs reveal that the choice of matrix density in the calculations is too low for the given occurrence and is approximated to ca. 0% in this study. This will be discussed further in Section 4.1.1. See supplements for the density, neutron-porosity, gamma-ray, and calculated porosity logs.

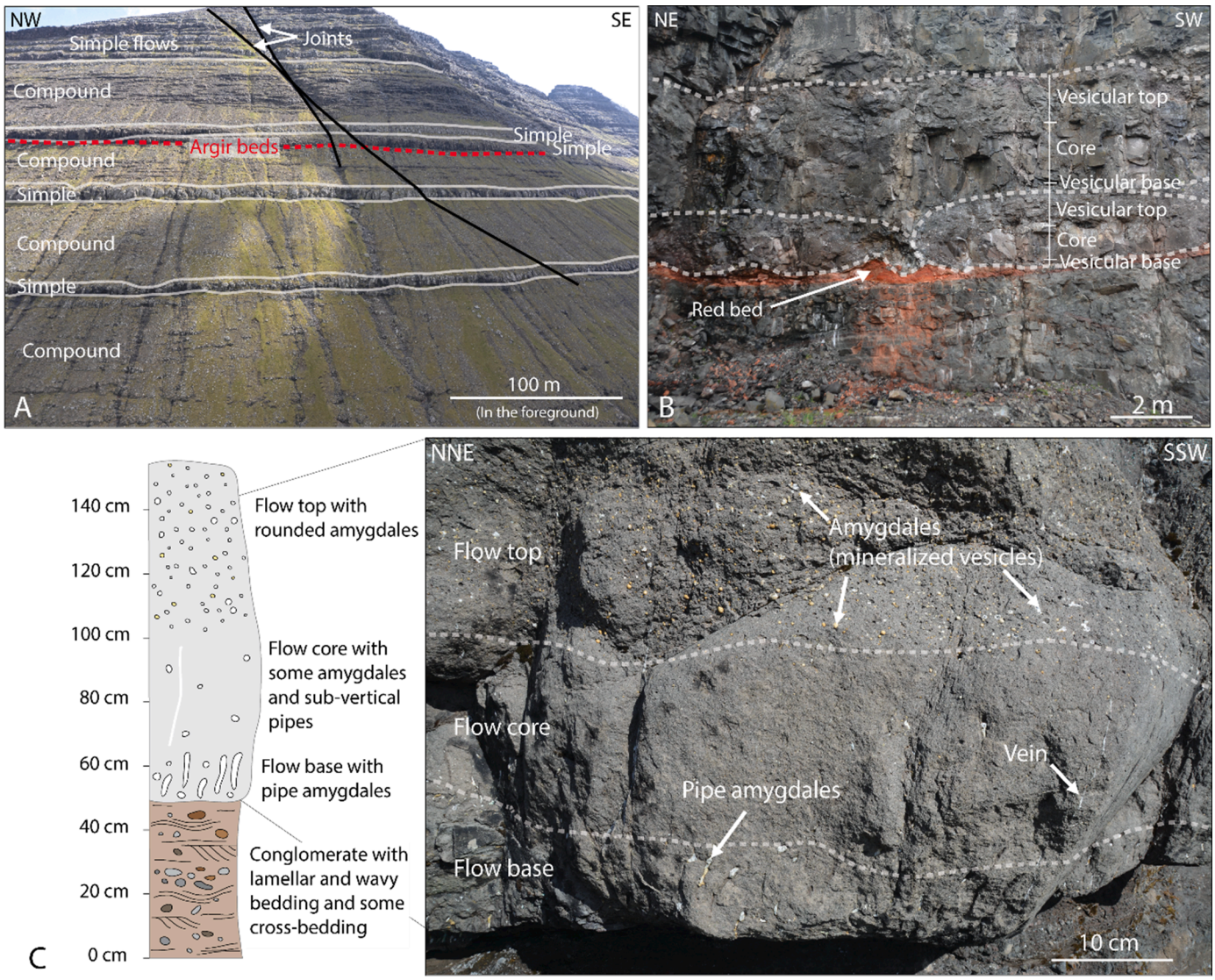

Fig. 3. Field observations from the upper FIBG stratigraphy. **A)** The Enni Mountain hillside at Locality 1 (Fig. 1). Simple and compound-braided lava flow packages in the Enni Formation are indicated in addition to two joints. The location of the Argir beds is taken from Millett et al. (2017). **B)** Compound-braided lava flows in the Malinstindur Formation, observed at Locality 3 (Fig. 1). The compound flow lobes are loading into an underlying sedimentary "red bed". Individual lobes are outlined, and the internal architectures of some of the lobes are marked. **C)** A small pahoehoe flow lobe in the upper Malinstindur Formation, at Locality 2. The internal flow architecture of the lobe is indicated in the picture and in the log to the left.

3.1.3. Petrography of samples

The optical microscopy and SEM studies reveal that the sampled lava flows in the two boreholes have a primarily porphyritic texture. The texture is generally fine-grained, holocrystalline, with trachytic or aphanitic type phenocrysts of plagioclase or olivine (Figs. 4A and B); the plagioclase being more common sometimes occurring as glomerocrysts. The groundmass of the samples is mostly devoid of olivine and dominated by plagioclase microcrystals (primarily labradorite) of acicular and subhedral laths and clinopyroxene (augite) with frequent ophitic texture (Fig. 4C). Iron oxides (Ilmenite and Ti-magnetite) and orthopyroxene are also present. Zeolites are the major secondary minerals filling the pores of the samples (Fig. 4D). Other pervasive types of secondary mineralization are K-feldspar, clays (chlorite and smectite), and quartz. The vesicles generally have a rim of either zeolites or clay, but most are completely mineralized. The fractures and vesicles can frequently be seen to have dark alteration halos around them. These zones contain more K-feldspar, ilmenite, and clays (chlorite and smectite; Fig. 4D).

The sampled volcaniclastic interbeds in the boreholes are composed of volcanic rock fragments, volcanic glass, plagioclase, clays (chlorite and smectite), and various forms of zeolites (Fig. 4E). The studied sediments display moderate sorting, and the grain size varies between coarse to fine sand with clay filling in the space between grains. The grains are mainly subrounded and dominated by altered volcanic clasts ranging from crystalline basalt to altered glass. Most abundant are the black volcanic glass, primarily interpreted as tachylyte although light yellow/brown glassy fragments interpreted as sideromelane are also present (Fig. 4E). Some of the samples from the Argir beds (S3; Fig. 2) also showed zeolite mineralization between the grains.

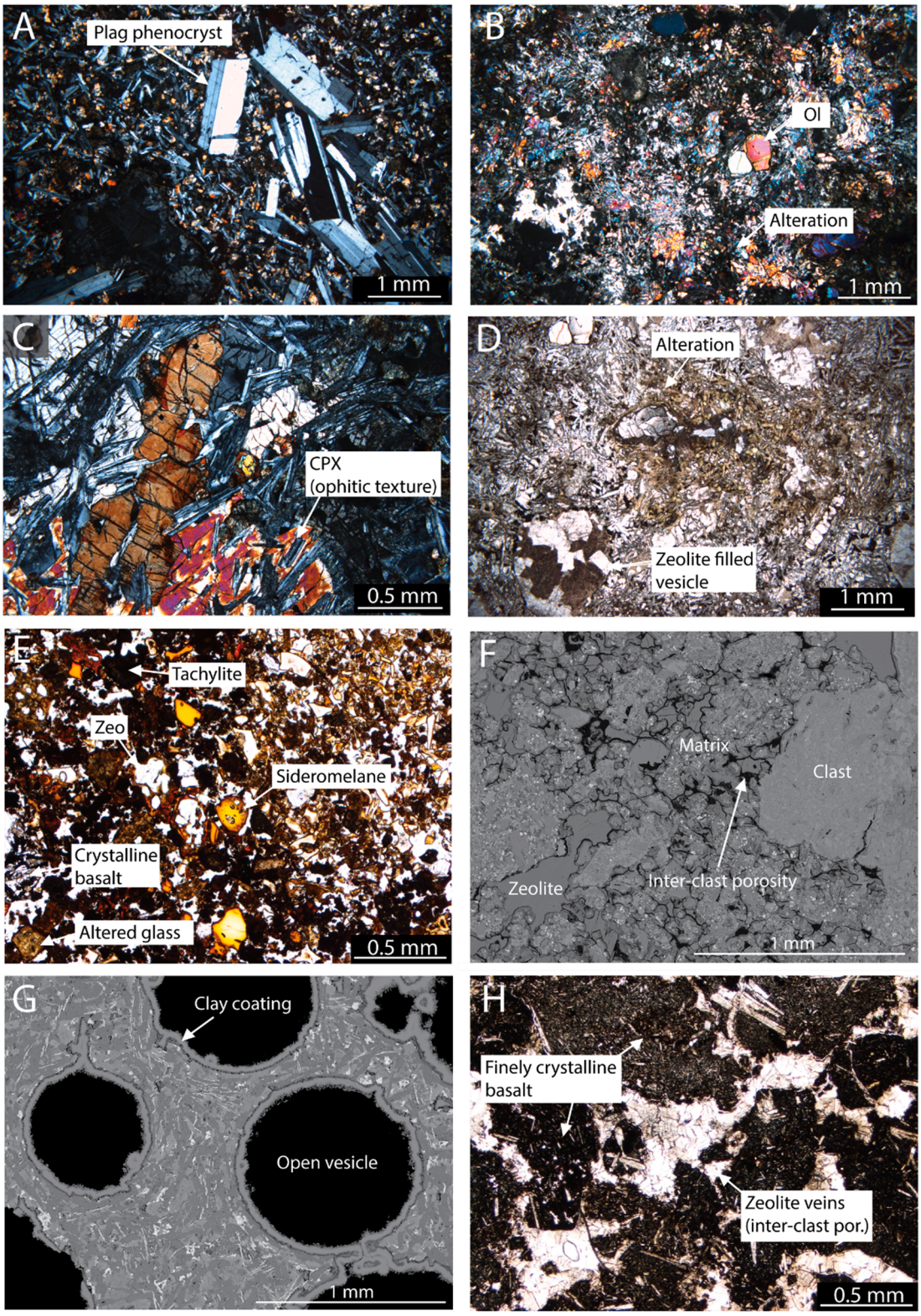

Fig. 4. Observations of the thin sections from the microscope with **A**) sample GM-17 thin section showing fresh plagioclase phenocrysts (in cross-polarized light), **B**) sample F20–09 thin section with fresh olivine phenocrysts adjacent to dark alteration zones (in cross-polarized light), **C**) sample F20–11 thin section displaying ophitic textures (in cross-polarized light), **D**) sample F20–09 thin section with distinctive green coloured alteration around a zeolite filled vesicle in the center of the image (in plane-polarized light), **E**) sample G_S3–1 containing volcaniclastic sediments from the Argir beds (S3) with zeolite cementation between the grains (in plane-polarized light), **F**) texture of the clasts and matrix in a BSE image of sample G_F3–1, with inter-clast or clast-supported porosity, **G**) sample G_F17–6 containing near-spherical vesicles that show a 0.1 mm clay coating, and **H**) sample Tj-2-FVII-4 from a volcanic breccia layer with finely crystalline volcanic clasts and zeolite veins (in plane-polarized light).

3.1.4. Internal architecture and petrography of case studies

Flows 3 and 4 in the Glyvursnes-1 borehole (case studies I and II; Fig. 2B) are both simple lava flows with a brecciated upper crust (Fig. 5). The flows display a traditional architecture with an upper and lower crust and a low-vesicularity core between (e.g., Passey and Jolley, 2009; Self et al., 1996; Walker, 1972). The presence of a brecciated upper crust and a vesicular lower crust for both flows are consistent with transitional rubbly pahoehoe to Aa lava flow facies. The breccia contains irregular, volcanic clasts with a microcrystalline to glassy texture (Fig. 4F). The matrix between the clasts is primarily microcrystalline in texture and dominated by smaller-scale clasts with common broken/collapsed vesicles at their margins (Fig. 4F). Larger-scale coalesced amygdales are observed in some clasts. The matrix reveals a well-connected inter-clast, or clast-supported, framework with additional intra-clast vesicular porosity, whereas only some of the vesicles in the clasts are seen to be connected in the thin sections (Figs. 4F). Most of the vesicles in Flow 3 are mineralized (Fig. 4F) while the vesicles in the Flow 4 top are primarily open and coated with clay minerals.

Flow 17 in the Glyvursnes-1 borehole (Case study III; Fig. 2B) is an example of a compound-braided flow and consists of 22 different flow

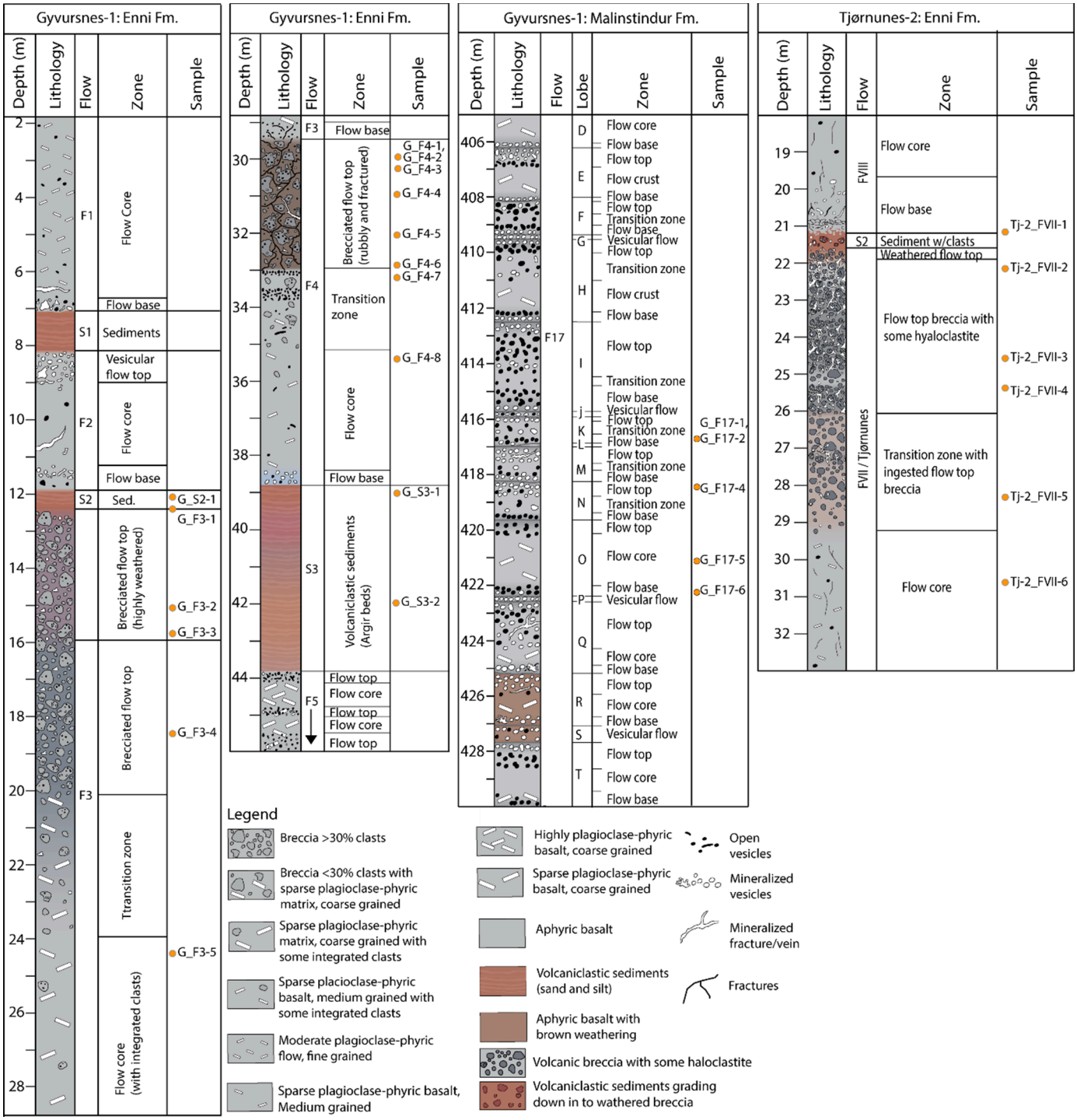

Fig. 5. Logs of case study intervals (flows 3, 4, and 17) from the Glyvursnes-1 core and the Tjørnunes-2 core (FVII) with lithology, flow name, flow architecture (zone), and sample location marked. The logs were made based on photos of the core.

Table 1
Porosity measurements from the Glyvursnes-1 and Tjørnunes-2 boreholes from the CT analysis. The sample volume, porosity type, depth, measured porosity, and connected porosity of the samples are listed. ROI = Region of interest/ sub-volume.

Borehole	Sample	Depth (m)	Lithology	Volume type	Porosity type	Porosity from CT (%)	Connected porosity from CT (%)	Average porosity from ImageJ (%)	Porosity from bulk density (%)
Glyv-1	G_S2–1	12.10	Volcaniclastic sediment	BSE image	Micro	–	–	9.41	–
	G_F3–2	15.10	Brecciated flow top filled with secondary minerals	Whole sample	Present-day	4.3	0.0	–	–
					Primary	29.1	24.3	–	–
	G_F3–4	18.45	Brecciated flow top filled with secondary minerals	Whole sample	Present-day	3.6	0.6	–	–
				ROI	Present-day	9.7	2.3	–	–
					Primary	34.7	32.6	–	–
	G_F3–5	24.40	Flow core	BSE image	Micro	–	–	3.0	–
	G_F4–1	29.90	Brecciated flow top, mostly open porosity	Whole sample	Present-day	12.7	6.6	–	7.9
				ROI	Present-day	22.7	20.8	–	–
	G_F4–2	29.95	Brecciated flow top filled with secondary minerals	Whole sample	Present-day	4.4	2.1	–	–
					Primary	13.5	9.9	–	–
	G_F4–3	30.30	Brecciated flow top, mostly open porosity	Whole sample	Present-day	9.9	6.3	–	18.8
				ROI	Present-day	12.7	6.3	–	–
	G_F4–5	32.10	Brecciated flow top, mostly open porosity	Whole sample	Present-day	–	–	–	21.2
	G_F4–6	32.85	Brecciated flow top, mostly open porosity	Whole sample	Present-day	36.2	24.5	–	–
				ROI	Present-day	30.3	28.8	–	–
	G_F4–8	35.40	Flow core	BSE image	Micro	–	–	1.9	–
	G_S3–1	39.05	Volcaniclastic sediment	BSE image	Micro	–	–	11.2	–
	G_F17–1	416.70	Vesicular flow top, mostly open porosity	Whole sample	Present-day	15.1	0.2	–	12.9
	G_F17–5	421.15	Flow core	BSE image	Micro	–	–	1.4	–
	G_F17–6	422.20	Vesicular flow top, mostly open porosity	Whole sample	Present-day	26.5	0.5	–	20.0
Tj-2	Tj-2-FVII-1	21.20	Volcaniclastic sediment	BSE image	Micro	–	–	8.6	–
	Tj-2-FVII-2	23.25	Volcanic breccia filled with secondary minerals	Whole sample	Present-day	0.8	0.2	–	–
					Primary	23.9	18.8	–	–
	Tj-2-FVII-3	24.50	Volcanic breccia filled with secondary minerals	Whole sample	Present-day	0.7	0.1	–	–
					Primary	44.9	42.2	–	–
	Tj-2-FVII-6	31.75	Flow core	BSE image	Micro	–	–	1.40	–

lobes (here named A-V) of a pahoehoe-type ranging in thickness from ca. 10 cm to ca. 2.5 m (Fig. 5). Most of the lobes contain a vesicular upper and lower crust with a low-vesicularity core separating them. The crusts vary from being dominantly unmineralized to being completely filled with secondary zeolite and clay minerals (Fig. 5). Most of the vesicles appear isolated in the thin sections (Fig. 4G), however, some are connected through pore throats via vesicle coalescence or microfractures.

A ca. 7 m thick breccia layer (Fig. 5; termed hyaloclastite by Jolley and Passey, 2012) is found at the top of the Tjørnunes Flow (FVII) in the Tjørnunes-2 borehole (Case study IV; Fig. 2C). The general character and distribution of the breccia including its transition down into and partial ingestion into the flow interior are conformable with a rubbly flow top, however, the presence of broken glassy shards may also indicate some water interaction during emplacement. The breccia sequence consists of moderately- to well-sorted volcanic breccia with angular to sub-rounded clasts of finely crystalline basalt and volcanic glass, welded together by a variably zeolite mineralized rock matrix of similar but finer-grained fabric (Fig. 4H). Clay coating is observed around the edge of vesicles and veins. There is very little open porosity present as most of the pore space has been mineralized.

3.2. Porosity estimates from the samples

Most of the porosity visible in the CT scans from the brecciated flow tops is seen in the clasts as the resolution is too low to observe any pores in the matrix. Very little open porosity is seen in the scans of the Flow 3 samples, as the pores are mostly filled with zeolites. Present-day porosities are measured to 4.3% and 3.6% for samples G-F3–2 and G-F3–4, respectively (Table 1). In contrast, most of the vesicles in the scanned samples from Flow 4 are unmineralized (Fig. 6A) and the measured present-day porosities range from ca. 4.4% to ca. 36.2% (Table 1). The primary porosity (porosity before the clogging) of the Flow 3 flow top samples, assuming all secondary minerals in the scans have filled open pore space, are estimated to 29.1% and 34.7% (Table 1). For the Flow 4 flow top samples, the primary porosity estimates range between ca. 9.9% and ca. 36.2% (Table 1). The porosity visible in the CT scans from the vesicular flow crusts of Flow 17 is restricted to the near-spherical, vesicles (Fig. 6B). The present-day porosities of the two scanned Flow 17 samples are found to be 15.1% and 26.5% (Table 1). As both samples contain little to no secondary mineralization, the primary porosity is estimated to be approximately the same as the present-day porosity. The flow top breccia samples from Flow VII in the Tjørnunes-2 borehole

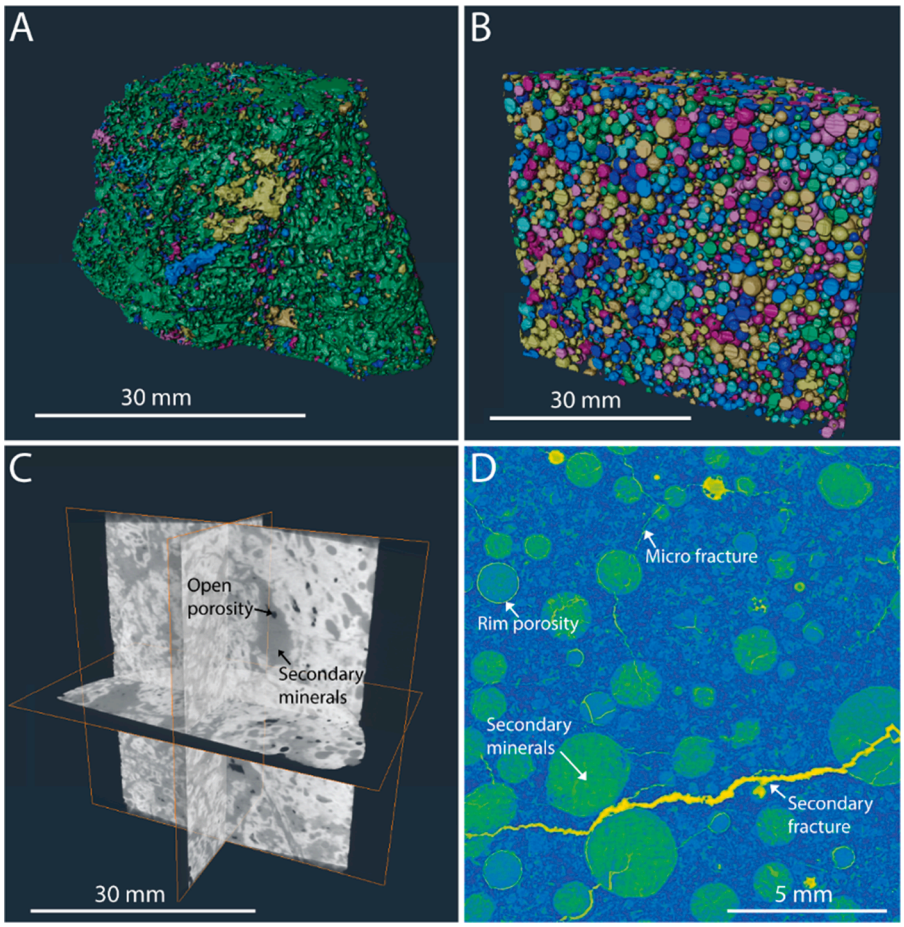

Fig. 6. Results from μ-CT image analysis show **A)** the separated open pore space from sample G_F4–6 (the brecciated flow crust sample with the highest porosity) with individual colours for each pore. Most of the porespace is found in one large pore, marked green. **B)** the separated pore space from sample G_F17–6 from a vesicular flow crust, **C)** the CT scan 3-D volume of sample Tj-2-FVII-3 with open porosity and secondary mineral phases marked, and **D)** the synchrotron scanned F20–10 sample from a mineralized vesicular flow top containing microfractures in and around the vesicles.

Table 2
Results from the permeability simulations of the three Glyvursnes-1 samples. The absolute permeabilities and flow rates per *sec*. in vertical and horizontal directions are listed for each sample.

Sample	Flow direction	Absolute permeability [k (m^2)]	Absolute permeability [k (D)]	Flow rate per *sec.* [m^3]	Depth (m)	Maximum pore radius (mm)	Maximum pore throat radius (mm)
G_F4–1	Vertical	3.8E-11	38.7	7.9E-06	29.9	2.3	0.9
	Horizontal	6.3E-11	63.9	3.9E-05			
G_F4–3	Vertical	3.2E-12	3.2	4.2E-07	30.3	1.2	0.8
	Horizontal	1.8E-11	18.7	9.6E-06			
G_F4–6	Vertical	8.7E-11	88.4	3.2E-05	32.85	1.3	1.2
	Horizontal	6.5E-12	6.6	2.5E-06			

contain almost no (<1%) open porosity (Fig. 6C; Table 1). The primary porosities are, however, estimated to ca. 23.9% and 44.9% for samples Tj-2-FVII-2 and Tj-2-FVII-3, respectively (Table 1).

Some inter- and intra-crystalline porosity is observed in the higher resolution synchrotron scans, but most prominent is the network of microfractures (Fig. 6D). Some of these fractures are very fine and reveal secondary mineral fills confirming their primary nature, whereas other small hair-line shrinkage cracks appear likely to be linked to shrinkage of originally hydrous secondary minerals during sample drying. Broader fractures crosscut the original and secondary mineral fabric are likely from the core extraction process (Fig. 6D). The microfractures are mainly restricted to vesicle edges or linking adjacent vesicles (Fig. 6D).

The ImageJ software analyses of color-coded chemical backscatter images give average flow core porosity for the two boreholes of ca. 1.93% with a standard deviation of 1.24%. The overall average sediment porosity for the borehole samples is 9.72% with a standard deviation of 1.75% (Table 1). The estimated porosity from the bulk density measurements for the brecciated flow top of Flow 4 is ca. 7.9%, ca. 18.8%, and ca. 21.2% for the samples G_F4–1, G_F4- 3, and G_F4–5, respectively (Table 1). The density estimated porosities for the vesicular flow crusts in Flow 17 are ca. 12.9% and ca. 20.0% for samples G_F17–1 and G_F17–6, respectively (Table 1).

3.3. Absolute permeabilities and connected porosities

The Flow 3 flow crust samples have present-day connected porosities of generally <1%, estimated from the CT scans. The primary pore spaces (before filling of secondary minerals) for samples G_F3-2 and G_F3-4 are

Table 3
BET specific surface areas (powdered samples), whole-rock geochemistry (oxides), and loss of ignition (LOI) for the reactivity samples.

Sample	Lithology	BET (m^2/g)	SiO_2	Al_2O_3	Fe_2O_3	MnO	MgO	CaO	Na_2O	K_2O	TiO_2	P_2O_5	LOI
GRM-01	Flow X core	*2.0*	*48.3*	*15.5*	*13.1*	*0.2*	*6.3*	*12.2*	*2.3*	*0.3*	*1.8*	*0.2*	*1.3*
GRM-02	Flow X brecciated top	*44.0*	*49.8*	*17.6*	*11.3*	*0.2*	*4.8*	*12.4*	*2.1*	*0.2*	*1.5*	*0.1*	*11.6*
GRM-03	Flow VIII core	*4.3*	*48.5*	*13.9*	*15.0*	*0.2*	*6.3*	*10.5*	*2.7*	*0.2*	*2.5*	*0.2*	*2.6*
GRM-04	Flow VIII vesicular top	*6.7*	*48.0*	*14.2*	*15.0*	*0.2*	*6.5*	*9.6*	*3.6*	*0.1*	*2.5*	*0.2*	*4.1*
GRM-05	Argir beds (S3)	*12.4*	*50.4*	*14.8*	*13.9*	*0.2*	*6.0*	*9.4*	*1.6*	*1.0*	*2.6*	*0.2*	*5.7*

Oxides are recalculated to 100 wt%.

estimated to have had a connected porosity of ca. 24.3% and ca. 32.6%, respectively. For Flow 4 the present-day connected porosities range from ca. 2.1% to ca. 24.5% while the primary connected porosities are estimated to have ranged from ca. 6.3% to ca. 24.5%. The present-day and primary connected porosities of the Flow 17 vesicular crust samples are estimated to be <1%. The same is found for the present-day connected porosities of the breccia layer in Flow VII. The primary connected porosities for samples Tj-2-FVII-2 and Tj-2-FVII-3 are, however, estimated to have been ca. 18.8% and ca. 42.2%, respectively. Three sub-volumes of samples G_F4–1, G_F4–3, and G_F4–6 were used to simulate fluid flow. The simulations gave absolute permeabilities ranging from ca. 3.2×10^{-12} m^2 (3.2 D) to ca. 8.7×10^{-11} m^2 (88.4 D) and flow rates through the samples ranging from ca. 4.2×10^{-7} m^3 /s to ca. 3.9×10^{-5} m^3 /s (Table 2). The maximum pore and pore throat radii found in the largest pore of the three sub-volumes were 2.3 mm and 1.2 mm, respectively.

3.4. Reactive surface areas and geochemistry

The powdered sample prepared from the brecciated upper crust of Flow X shows the largest specific surface area defined by Brunauer–Emmett–Teller-theory (BET) with a value of 44.0 m^2/g (Table 3). The smallest specific surface area is measured for the sample from the Flow X core with a value of 2.0 m^2/g. Even though some of this difference might stem from the preparation and cleaning of the powdered samples, both flow core samples show smaller surface areas than their related flow top as would be anticipated. The powdered sedimentary sample has the second-largest measured specific surface area of 12.4 m^2/g, albeit 3.5 times smaller than for the Flow X top. Throughout the kinetic experiments, no secondary minerals were observed within the outlet filter nor on the surfaces of the grains following the completion of the experiments. The grains are smaller and more rounded after the kinetic experiments, with the samples from Flow VIII (GRM-03 and GRM-04) showing the least change in size. The brecciated flow crust sample (and to some degree the volcaniclastic sediment) displayed poorer sorting and more angular grains after the experiments. See supplements for before and after images of the grains used in the experiments.

The amount of SiO_2 in the samples ranges between 44.2 and 48.3 wt %, and the contents of K_2O, Na_2O_3, P_2O_5, and TiO_2 vary the most. All samples classify as basaltic in composition, and all have high Titanium (High-Ti) affinity in comparison to other Faroe Islands basalts (Millett et al., 2017). Total divalent cation oxide concentrations (CaO, MgO, and FeO) within the samples range between 28.5 wt% (for GRM-05) and 31.8 wt% (for GRM-03). The loss on ignition (LOI) is highest for sample GRM-02 at 11.6% and lowest for GRM-03 at 2.6%.

Differences in Al/Si, Fe/Si, and Mg/Si ratios between the flow top and flow core samples from Flow X are observed (Fig. 7). This is not seen for the two other genetically related samples from Flow VIII, which share very similar elemental ratios. The samples can be divided into two groups based on their concentration of light rare earth elements (LREE) relative to the heavy rare earth element (HREE) concentration (Fig. 7). The inter-lava bed (GRM-05) and Flow VIII samples make up Group 1 with higher LREE/HREE ratios, while the Flow X samples make up Group 2 with lower LREE/HREE ratios. GRM-02 shares an almost identical elemental ratio profile to GRM-01, albeit with lower values, a result of LOI discrepancies. The samples represent aphyric and plagioclase phyric types with their mineralogy and modal abundances listed in Table 4. The chemical variability within the reactivity samples shows more plagioclase of lower An-composition within Flow VIII compared to Flow X, with the addition of plagioclase andesine, which is still minor compared to plagioclase labradorite. Flow X differs with more An-rich plagioclase with minor amounts of plagioclase bytownite.

3.5. Dissolution rates

From the kinetic reactivity experiments, BET surface area normalized rock dissolution rates were calculated as Si release rate in $mol/cm^2/s$ (Supplements, Fig. 8A). After more volatile dissolution rates during the early stages of the experiments, steady-state conditions are achieved after ~450 h in the mixed-flow experiments; however, for the brecciated flow crust sample (with the highest BET; GRM-02) steady-state condition was achieved faster, at ~100 h (Fig. 8A). Dissolution rates are similar for the flow cores, whereas the flow tops show a significant difference, with the vesicular crust from Flow VIII (sample GRM-04) expressing faster dissolution rates than the brecciated flow crust of Flow X (sample GRM-02). The steady-state profiles show the flow core of Flow X (sample GRM-01) to have a slightly higher dissolution rate than the flow core of Flow VIII (sample GRM-03). This is followed by the vesicular flow crust sample (GRM-04), the brecciated flow crust sample (GRM-02), and the volcaniclastic sediment sample (GRM-05), respectively (Fig. 8A). The relative mobility of elements Al, Ca, Fe, K, Mg, and Na (i.e., their release rates relative to their abundance in the solids and compared to Si, see Supplements) were plotted as a function of time (Fig. 8B). There is a preferential release of K and Al, close to stoichiometric release for Ca, and preferential retention of Mg and Fe. The volcaniclastic sediment sample shows a different trend with Mg being preferentially retained up to ~280 h, where it becomes preferentially released, although close to stoichiometric levels. Ca release rates relative to the total release rates of divalent metal cations within the rocks are shown to be between 64 and 97%, whereas Mg ranges between 0 and 34% and Fe from almost 0 to 19%. Hence, Ca^{2+} represents the most significant divalent metal cation being released (Fig. 8B).

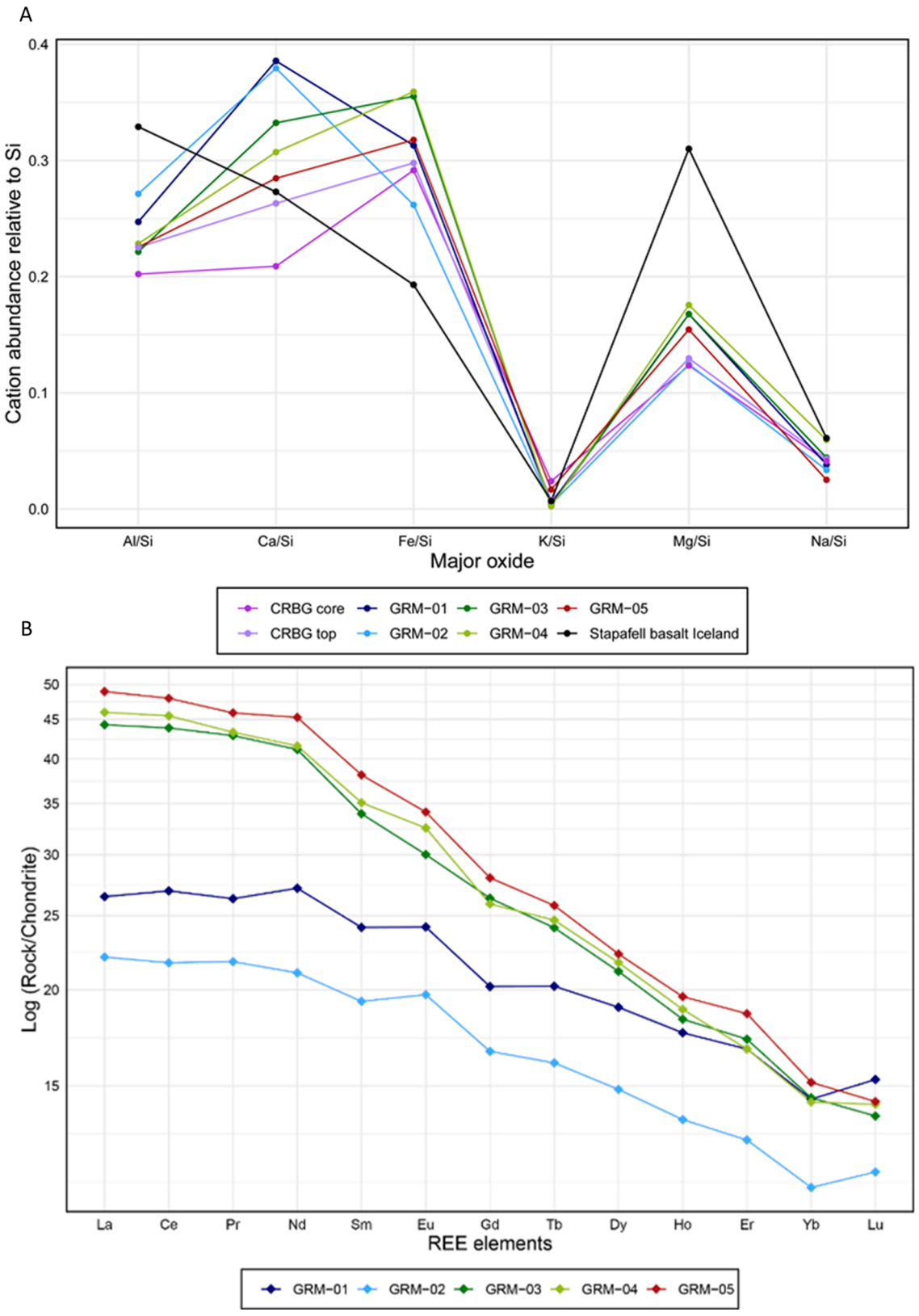

Fig. 7. Results from whole-rock geochemistry. **A**) Cation concentrations relative to Si within the dissolution samples (weight%). Most samples share similar profiles, albeit GRM-02 shows an elevated Al ratio and lower Fe and Mg ratios. The bulk rock concentrations relative to Si for the Faroe Islands rocks show that the Icelandic basalt (Stapafell Mountain Dyke in Iceland -SMD) has significantly more Mg (numbers from Schaef and McGrail, 2009). **B**) REE plot from Inductively coupled plasma mass spectrometry (ICP-MS) results on reactivity samples GRM-01 to GRM-05 showing the elements normalized to chondrite values taken from Sun and McDonough (1989). GRM-02 shares a very similar profile to GRM-03, just lower due to LOI. GRM-01 = Flow X flow core, GRM-02 = Flow X brecciated flow top, GRM-03 = Flow VIII flow core, GRM-04 = Flow VIII vesicular flow top, GRM-05 = Volcaniclastic sediment (Argir beds), and CRBG = Columbia River Basalt Group.

Table 4
Mineral modal abundances of the kinetic experiment samples.

Mineral	Chemical formula	GRM-01 (%)	GRM-02 (%)	GRM-03 (%)	GRM-04 (%)	GRM-05 (%)
Ca-rich Plagioclase	$CaAl_2Si_2O_8$	*62.6*	*34.2*	*47.0*	*24.6*	11.4
Clinopyroxene	$(Ca,Mg,Fe)Si_2O_6$ (monoclinic)	*27.2*	*18.2*	*24.1*	*18.4*	15.5
Orthopyroxene	$(Ca,Mg,Fe)Si_2O_6$ (orthorombic)	*3.0*	–	*5.5*	*1.2*	–
Ti-magnetite	$Fe^{2+}(Fe^{3+},Ti)_2O_4$	*3.1*	*4.5*	*2.7*	*2.5*	0.9
Glass	Large variations in composition	–	–	–	–	19.6
Zeolites	$(Ca,Na_2)Al_2Si_4O_{12} \times 6H_2O$ (for chabazite, several variations of zeolites do however occur)	*1.0*	*34.0*	*10.2*	*27.8*	24.3
Na-rich plagioclase	$NaAlSi_3O_8$	–	*3.8*	*8.4*	*23.0*	–
K-feldspar	$KAlSi_3O_8$	*1.0*	*2.2*	–	–	0.5
Ilmenite	$(Fe,Ti)_2O_3$	*1.5*	–	*1.9*	*1.6*	–
Smectite/chlorite	–	*0.6*	*3.2*	*0.3*	*0.9*	27.6

4. Discussion

Large variations in reservoir properties are expected in the studied volcanic sequences as the vertical heterogeneity of the lava flow domains and inter flow layers is significant. A 10 m interval of the Glyvursnes-1 core might contain several crusts (of high or low permeability), low permeability cores, and sedimentary interbeds. A single flow top or base may also contain zones of open porosity and zones of mineralized rock. There are also horizontal variations in reservoir properties that will affect fluid flow (e.g., intrusions, faults, or facies variations). The mechanism that contributes most to fluid flow may differ between zones, often varying between being vesicle dominated in the flow crusts and fracture dominated in the flow cores. Better constraints on the spatial variability of the reservoir properties in basaltic lava flows and the main contributing fluid flow factors are needed (Burns et al., 2012; Jayne et al., 2019).

4.1. Porosity and permeability in the volcanic sequences

4.1.1. Comparison between porosity logs and laboratory measurements

Calculating porosity from the density log has limitations. The density of the flow core intervals used to calculate the matrix density of the least altered basalt varies between ca. 2.65 g/cm3 and ca. 3.0 g/cm3, likely because of local rock alteration leading to secondary mineralization (Japsen et al., 2006). Using a matrix density of 2.85 g/cm^3 for the Φ_1 log gives more conservative porosity estimates for the least altered basalts than using the highest matrix density of around 3.0 g/cm^3. A problem that arises from the conservative choice in matrix density is that the Φ_1 log predicts porosities below 0% in the least altered basalts, usually the flow cores (Section 3.1.2), which is not physically possible. This confirms that the matrix density is higher than the model for these intervals. However, a higher matrix density leads to an overall overestimation of flow crust porosities, which comprise the intervals of most interest for this study. The negative modelled porosities for the flow cores are associated with the predictably low porosity nature of the flow cores. Errors in the density log may also arise if, e.g., the borehole walls are too rough or the borehole is too large locally, more likely to occur in the sedimentary interbeds in the borehole (Broglia and Ellis, 1990; Schlumberger, 1987). The effect of this would be too high calculated porosities in certain sedimentary intervals.

The porosity measurements from the laboratory work were plotted together with the two end-member density-based porosity logs, the neutron porosity log (NPHI), and the lithological logs for the three sample intervals in the Glyvursnes-1 well (Fig. 9). The CT-derived porosities from the flow crust that are clogged with zeolite minerals (Flow 3 and the top of Flow 4) generally fit the Φ_2 log, for sediments and altered crusts, quite well (Fig. 9). The Φ_1 log (for the least altered basalt) fits the porosity measurements (CT and bulk density) for the mainly unclogged crusts in flows 4 and 17, and the ImageJ estimates of flow core porosities (Fig. 9). The ImageJ porosity measurements for the sedimentary layers give slightly lower estimates than the Φ_2 log (Fig. 9). Porosity (He porosity) data from Ólavsdóttir et al. (2015) were, therefore, plotted together with the lab results and seen to fit the Φ_2 log quite well (Fig. 9). These minor differences can be easily explained by the relatively small scale of the different samples and the heterogeneity of the volcaniclastic units. The Φ_2 log gives a reasonable estimate of the porosities in the sedimentary interbeds in the Glyvursnes-1 borehole, which it should, given the dominantly altered and consistent nature of the volcanic grains and grain densities.

The gamma-ray (GR) log has on occasion, been used to estimate the clay proportion in volcanic sequences assuming an average content of radioactive elements in clay (Barton et al., 1989; Broglia and Moos, 1988). If the GR log reflects the degree of alteration in the volcanic sequences, it could be used to calibrate the porosity log and choose a fitting matrix density for each interval. However, no direct and consistent connection between the GR log and internal flow architectures of the basalt flows, which should then be seen, was observed. The likely cause of this is that the GR log shows varying results for different types of clay, independent of the amount (Planke, 1994). Where geochemical logs are available (e.g., Zakharova et al., 2012), there is the potential to try and track alteration and use this to calibrate porosity models, however, these logs are not always available and may require core calibration to use effectively.

4.1.2. The volcanic breccia

The CT image analyses estimate a very low porosity (<5%) in the mineralized brecciated flow crust of Flow 3 in the Glyvursnes-1 borehole and Flow VII in the Tjørnunes-2 borehole. In contrast, the brecciated flow top of Flow 4, containing mainly unclogged vesicles, has measured porosities from the laboratory analyses up to ca. 36.2%. The brecciated crusts, therefore, seem to have a potentially high porosity if the pores have not been mineralized. This is supported by the fact that the primary porosities of the brecciated flow crust samples are estimated to have ranged from ca. 10% to ca. 45% before mineralization of the pore space. From the SEM studies of the volcanic breccia in Flow VII, it was apparent that most of the secondary minerals (and, therefore, likely the primary pore space) were present between the clasts. The highest estimates of primary porosity for the volcanic breccia (44.9%), therefore, include the inter-clast porosity that may be present where the space between the rubble has not been filled.

The present-day connected porosity for the clogged upper crust of Flow 3 and volcanic breccia from Flow VII suggests, unsurprisingly, very low permeabilities in these layers (<1% connected pore space). The connected porosities of the Flow 4 top crust samples range from ca. 2.1% (for the clogged samples) to ca. 28.8% (for the unclogged samples). The permeability can evidently range from very low to very high within the same crust, depending on the degree of secondary mineralization. The highest simulated permeability reached up to ca. 88 D, for the most

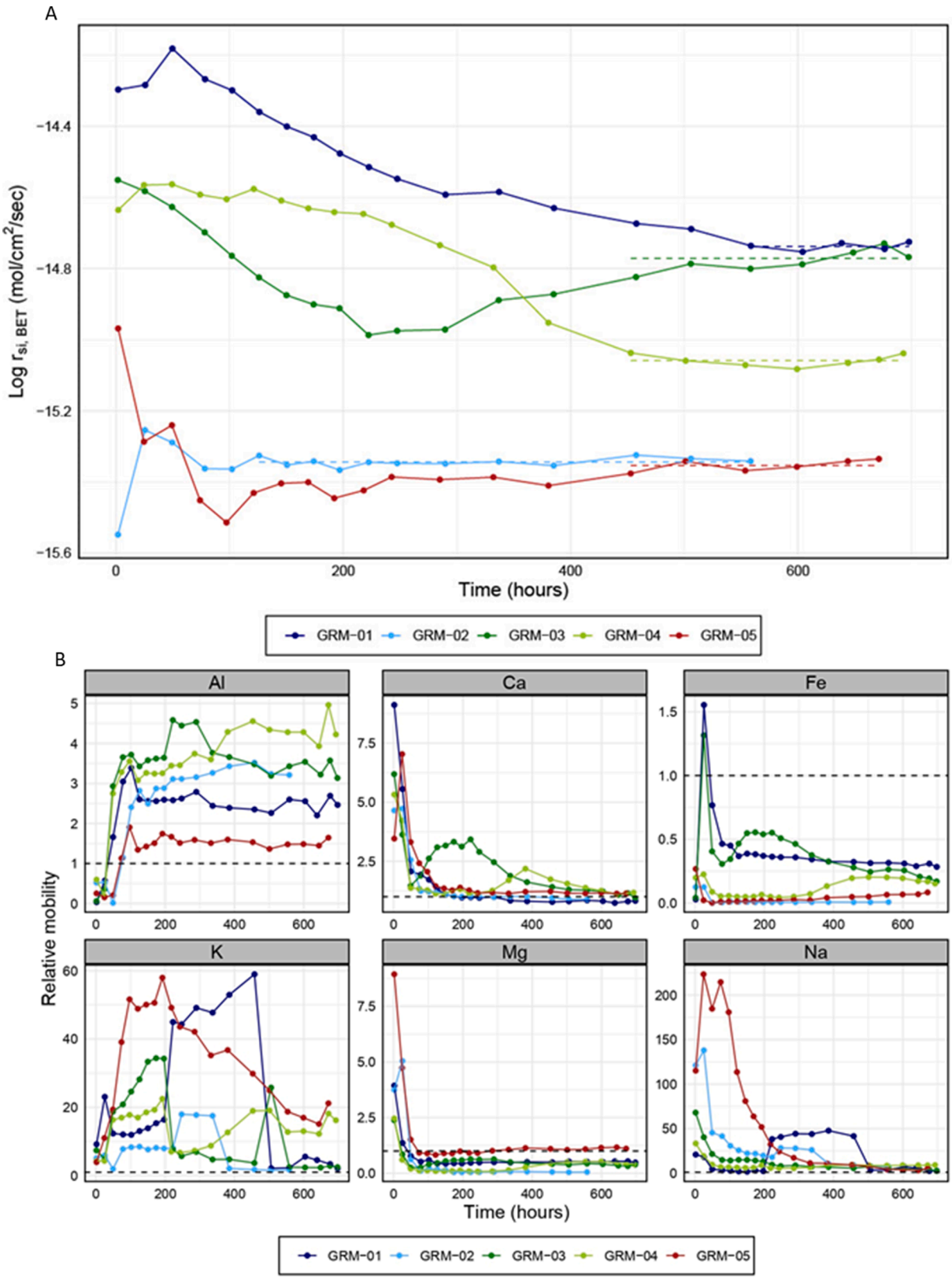

Fig. 8. Results from the kinetic experiments. **A**) Dissolution rate versus time for each sample. The experiments were run at pH 4 and 25 °C for over ~700 h when all the rocks reached a steady-state dissolution rate shown by a flat projection (dotted line). At first, the rocks show a more volatile dissolution rate before reaching a steady state. **B**) Relative mobility of elements vs time. A relative mobility of 1 (dashed line) illustrates the stoichiometric release relative to Si for a particular sample; if the relative mobility is <1 the element is preferentially retained relative to Si, whereas if the relative mobility is >1, the element is preferentially released relative to Si. See supplements for exact numbers.

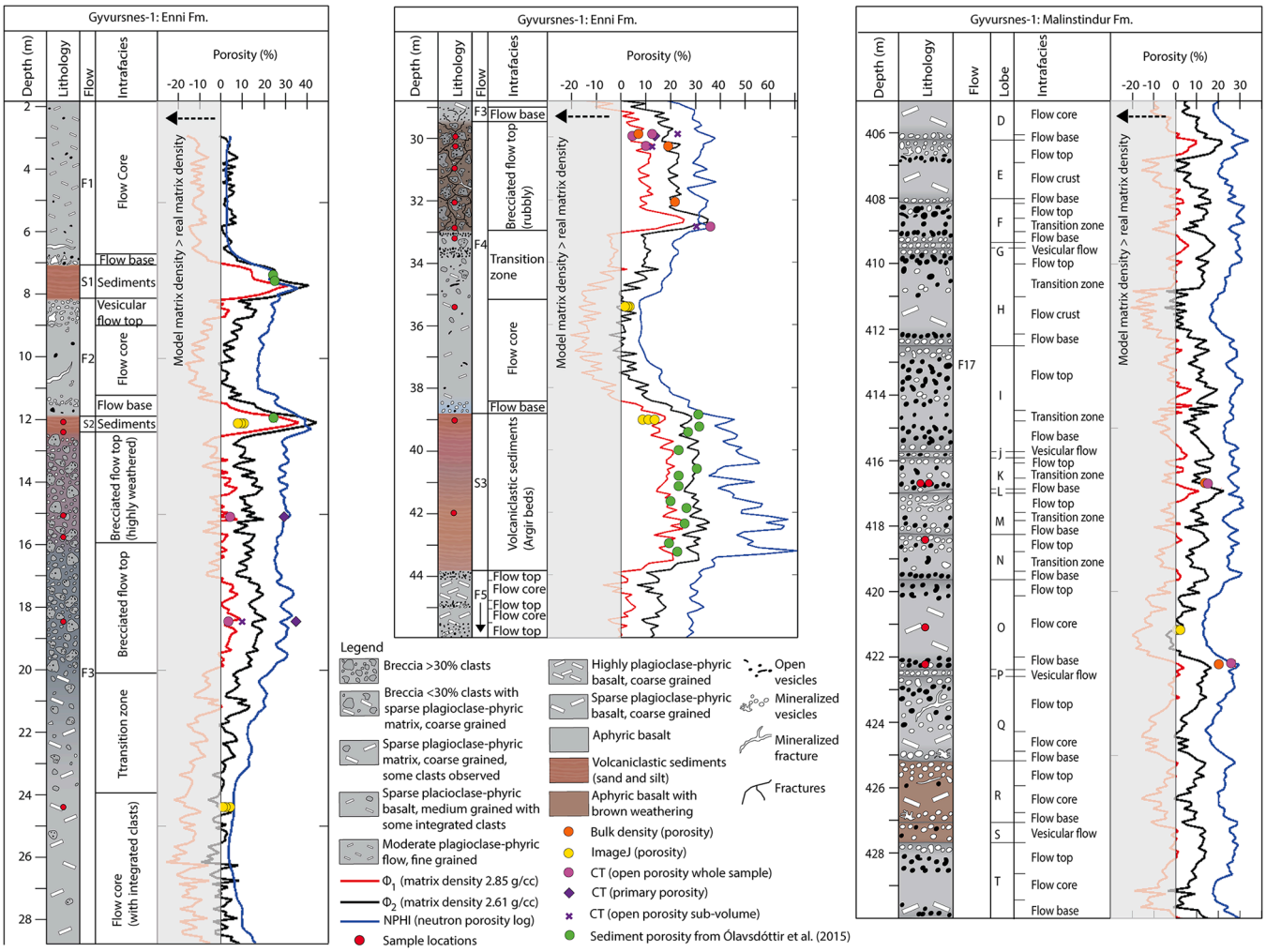

Fig. 9. Sample intervals from the Glyvursnes-1 borehole with the calculated porosity from the density log (Φ_1 and Φ_2 for a matrix density of 2.85 g/cm3 and 2.61 g/cm3, respectively), the neutron porosity log (NPHI), and porosity measurements from the samples using ImageJ, CT, density measurements and Ólavsdóttir et al. (2015) plotted together.

porous (unclogged) sample from the Flow 4 crust. However, it is likely that the true permeability of this rock would be significantly lower if injected with dissolved CO_2. Callow et al. (2018) showed that the measured permeability of basalt from hydromechanical tests was up to four orders of magnitude lower than what simulations using the Avizo software indicated. They suggest the cause of this to be the presence of swelling clays (particularly from smectite) in the vesicles. All the studied flow crust samples from the Glyvursnes-1 borehole contain significant clay coating in the vesicles and fractures. This could push the permeability values for the flow top of Flow 4 below 10 mD resulting in low permeability (Selley, 1976). The simulations do, however, show that there are potentially highly connected pore networks in the brecciated flow crusts. The connected porosities of the breccia samples are estimated to range from 6.3% to 42.2% in the primary pore space suggesting an initially well-connected pore network in most of the volcanic breccia samples, before clogging by secondary minerals.

Callow et al. (2018) state that errors in choosing one sample volume over another should be neglected because pores occur randomly in basalt. This might, however, not be the case in, e.g., the volcanic breccia, as the largest pores are more likely to occur in the clasts than in the matrix. Many of the sub-volumes in the CT scans were from the most porous clasts, which generally show higher macro-porosity values than for the scan of the whole sample. The primary porosity of the samples was estimated from the combined open porosity and mineralized pore space in the CT scans. This method does not consider the weathering of the minerals, e.g., in the groundmass or on the surface of vesicles, which might lead to an overestimation of the primary porosity.

4.1.3. The vesicular basalt

The vesicular flow crusts in Flow 17 have estimated porosities for the two crust samples between ca. 12.9% and ca. 26.7%. These samples contained almost only open vesicles and are therefore likely examples of the highest porosities present in this flow. The vesicular flow crust samples display extremely low connected porosities (<1%), a feature that is not uncommon for vesicular rocks with porosities below ~29%. The percolation threshold describes the minimum porosity threshold needed to create connected paths in the pore space through the rock (Kirkpatrick, 1973; Mavko and Nur, 1997). According to Rintoul and Torquato (1997), a connected network of random, equal-sized spherical pores in a vesicular material will have a percolation threshold of around 29% porosity. The two samples from Flow 17 are below this threshold, but as seen from the density log-derived porosities, vesicular flow tops in the Malinstindur Formation in the Glyvursnes-1 flow may reach above it (up to ca. 50%). In addition, the SEM analysis and higher-resolution CT scans showed that microfractures connect some of the vesicles in these crusts.

4.1.4. The flow cores and volcaniclastic red beds

Both the results from the laboratory analyses and the porosity log show that the porosities of the lava flow cores are low (<5%). Generally,

the present-day and primary porosity and permeability of the flow cores are low and in many cases form sealing rocks in the sub-surface (Burns et al., 2012). In contrast, the Φ_2 log gives conservative estimates of potentially high porosities (up to ca. 35%) for the volcaniclastic interbeds in the Enni Formation of the Glyvursnes-1 borehole. A decrease of up to 20% in porosity (to maximum ca. 15% porosity) from the top to the base of the borehole is seen. This is likely the cause of mechanical and chemical compaction (Lundegard, 1992). The permeability of the volcaniclastic beds studied in the Glyvursnes-1 and Tjørnunes-2 boreholes were estimated from the optical microscopy and SEM studies since the size of the pores was too small (often <0.1 mm) to be detected in the CT scans. A high clay content in these sediments suggests a low permeability (e.g., Planke, 1994).

4.2. Geochemistry and reactivity

4.2.1. Basalt and sediment reactivity

The results from the kinetic experiments demonstrated that flow cores have greater BET normalized dissolution rates than corresponding flow tops. The additional differences in dissolution rates between lava flows and inter-lava sedimentary beds support the idea that the mineral assemblage and the mineral's intrinsic dissolution rates control the dissolution rates of the entire system (Gudbrandsson et al., 2011). The flow tops have experienced more alteration than the flow interiors, as can be seen by the divalent metal cation release rates. The flow tops show 2.3- and 141-times lower Fe release than the corresponding flow cores. According to Schaef and McGrail (2009), this is likely a consequence of the low solubility of Fe^{3+} within the alteration products in these crusts. This also suggests that the alteration within the top of Flow VIII is less extensive than in Flow X. Moreover, the inter-lava bed shows the slowest Fe release rate of the samples, indicating that Fe^{3+} is dominant in this sample (Schwertmann, 1991). The Fe component of the rocks from the Faroe Islands is, however, low compared to Ca and Mg and thus the oxidation of Fe^{2+} to Fe^{3+} will have limited influence on carbonate formation.

The comparison between the divalent metal cations indicates that Ca^{2+} is the dominant cation released during the dissolution of the Faroe Islands rocks. The release rate of divalent metal cations would control the type of carbonate mineral precipitation during CO_2 storage and suggests that calcite or aragonite precipitation would be favoured, depending on the chemical and physical conditions (e.g., Gysi and Stefánsson, 2008; Tutolo et al., 2021; Voigt et al., 2021). This study has found the relative mobility of Ca during the dissolution of each sample to show an inverse relationship to the overall rock dissolution rates (i.e., Si release rates). This may reflect a positive correlation between the amount of secondary mineralization and the Ca^{2+}release rates, supported by the fact that the core of Flow X contains the most Ca but shows the lowest release rate of Ca^{2+}. As zeolites dominate the secondary mineralogy in the reactivity samples, the high Ca^{2+} release rates are likely caused by dissolving of these minerals. Although zeolites show slow normalized dissolution rates, they have substantial surface areas and therefore provide significant cation contributions (Kesraoui-Ouki

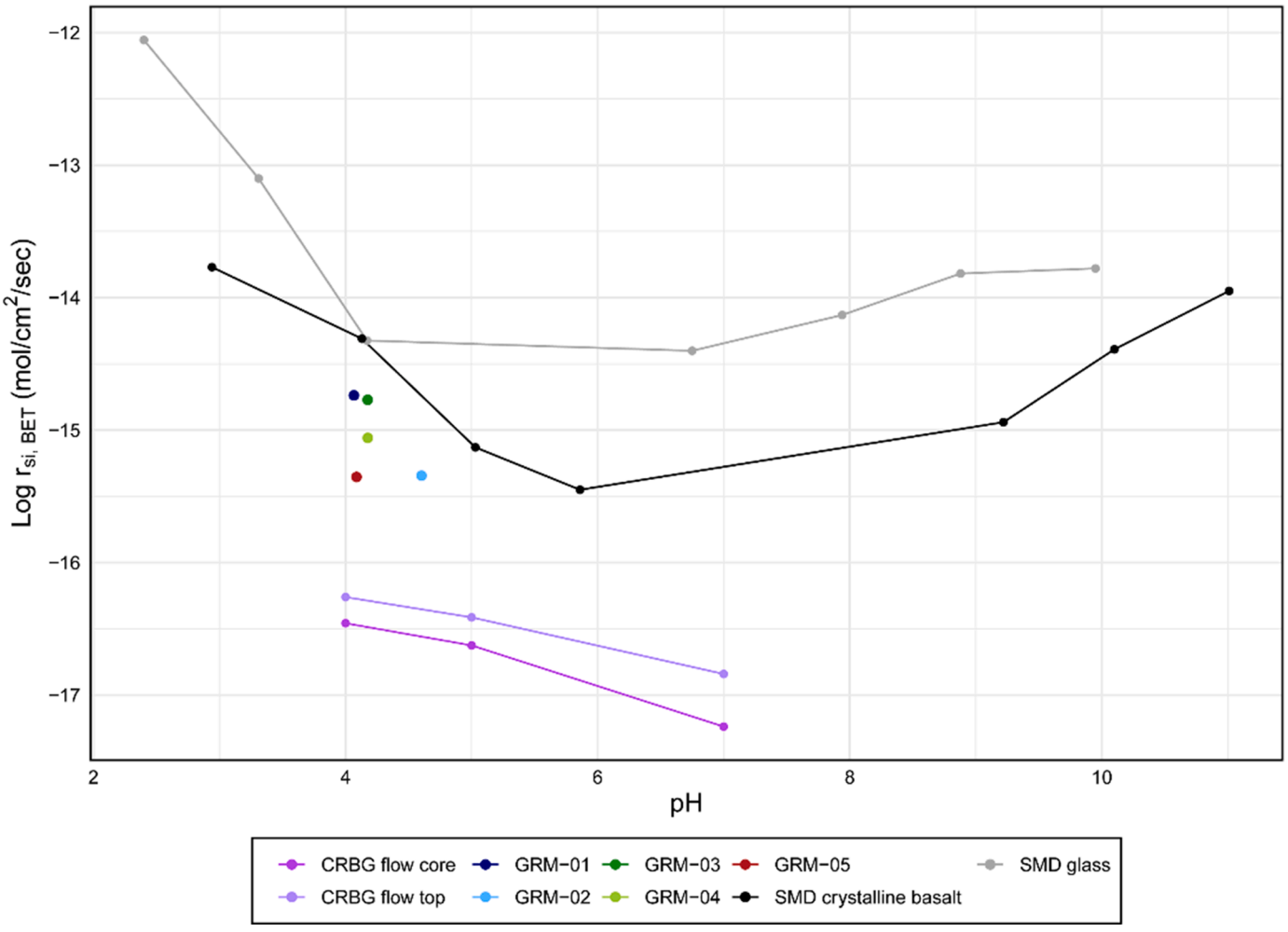

Fig. 10. Comparison between the steady-state dissolution rates of the five field samples from this study and the experimental results of Schaef and McGrail (2009) and Gudbrandsson et al. (2011) at 25 °C. Stapafell Mountain Dyke in Iceland (SMD). Columbia River Basalt Group (CRBG) in th US.

et al., 1993) and could enable fast CO_2 mineralization.

This study found the reactivity of the inter-lava bed to be slower than the basalt samples. The volcaniclastic bed contains a significant proportion of volcanic glass, which is expected to increase dissolution rates (Gudbrandsson et al., 2011). However, the volcanic glass is typically devitrified indicating that these reactions have already taken place and extensively limiting its reactivity. The volcaniclastic sediments will, however, have a considerably higher reactive surface area than the basalts in uncrushed samples potentially elevating the overall dissolution rate per reservoir volume in natural settings.

4.2.2. Comparison with rocks from Iceland and CRBG

The dissolution rates derived from the kinetic experiments give insights into the first stage of the carbon mineralization processes, i.e. the release of cations from the rock at pH similar to that of CO_2-charged water. However, dissolution rates derived from the kinetic experiments using powdered material are not a direct measurement of absolute rates in the reservoir and would need to be combined with the unknown in situ reactive surface area. Therefore, the most meaningful comparison is that to similar experimental results of basalts from the Wallula and Carbfix injection sites where successful CO_2 mineralization is documented (Fig. 10; Gudbrandsson et al., 2011; Schaef and McGrail, 2009). The samples studied here have only slightly lower dissolution rates than those of the Carbfix injection site and significantly faster rates compared to the Wallula CRBG basalts. This suggests that initial dissolution reactions are sufficiently fast to enable rapid mineralization in the formations studied here.

Differences in steady state dissolution rates are likely caused by varying mineralogy and initial basalt chemistry. The Icelandic rocks contain olivine, which dissolves significantly faster than other common basaltic minerals (Barnes and O'NEIL, 1969; Kelemen et al., 2018; Kelemen and Manning, 2015; Seifritz, 1990), whereas the High-Ti lava flows of the Faroe Islands are devoid of olivine, explaining the slower bulk dissolution rate for these rocks (Fig. 10). The CRBG basalts are also devoid of olivine and have lower dissolution rates than both the Icelandic rock and the FIBG rocks (Fig. 10). Part of the difference may also be due to a somewhat more Na-rich plagioclase in the CRBG basalts (Gudbrandsson et al., 2014).

As reactions progress in real injection scenarios, pH increases beyond the pH of ~ 4 studied in the experiments (e.g. Wolff-Boenisch 2011). The data from Gudbrandsson et al. (2011) and Schaef and McGrail (2009) shows a pH dependency on Si release which was not investigated in this study, but it appears reasonable to assume a resembling pH dependence to the similar Iceland basalts, supported by the results of Pollyea and Rimstidt (2017) modeling the dissolution rates of crystalline and glassy basalt with changing pH.

In this study, only the dissolution rates of olivine-free High-Ti lava flows were investigated. Since the Low-Ti flows, which become volumetrically important towards the top of the Faroe Islands and East Greenland sequences, commonly contain abundant olivine, their reactivity is expected to be greater than the tested High-Ti rocks (Millett et al., 2017). Moreover, only a single sample from the Argir Beds volcaniclastic unit was tested for dissolution rate in this study. This unit is interpreted as a fluvial deposit and the common occurrence of fallout ashes and other volcaniclastic lithologies, seen separating many of the lava flows in the province, require further and more comprehensive testing for differences in dissolution rates (Ólavsdóttir et al., 2015).

4.3. Potential reservoirs and caprocks

4.3.1. Reservoirs

The most porous and permeable rocks are likely found as volcanic breccia (e.g., flow crust breccia) that has not undergone mineralization. Brecciated flow crusts were also the main injection target in the Wallula pilot project in the CRBG (McGrail et al., 2011). The vesicular basalts (vesicular crusts) display a potentially high porosity but an often poorly connected pore network unless the porosity reaches above the percolation threshold of 29% (Rintoul and Torquato, 1997). Previous studies of vesicular flow crusts have shown that these rocks may be highly permeable (Callow et al., 2018; Couves, 2015; Saar and Manga, 1999). The least altered flow crusts will be the most reactive in contact with CO_2 as the altered crusts often display slower dissolution rates, but more importantly low porosity and permeability due to clogging of the pores. Zeolites may contribute significant amounts of Ca^{2+} for carbonate mineralization in altered crusts. However, the rocks with a large degree of zeolite mineralization were seen to be low in porosity and permeability lowering the surface area available for reactions. Still, these clogged rocks may present additional reactive material if the CO_2 migrates away from the primary fluid pathways and into the surrounding host rock over time.

Most of the pores and pore throats in the pore network models of the samples were <1 mm in radius. This implies that the pore networks in the clasts of the brecciated flow tops are vulnerable to clogging by the precipitated minerals, e.g., when reacting with CO_2 (Callow et al., 2018; Van Pham et al., 2012; Wolff-Boenisch and Galeczka, 2018). However, mineralization may also induce micro fracturing and promote CO_2 migration through the rock (Kelemen et al., 2013; Røyne et al., 2015; Zhu et al., 2016). Dissolution of the different Fe, Mg, and Ca-bearing minerals in the rock can also enhance the porosity and permeability, counteracting the clogging effect (Matter et al., 2009).

4.3.2. Caprocks

The calculated porosity logs and the SEM studies of the basalt flow cores indicate very low porosities (generally <5%). Some fracture-controlled, fluid flow through the flow cores may occur (Aradóttir et al., 2012; Snæbjörnsdóttir et al., 2018; Zakharova et al., 2012). However, secondary mineralization would effectively clog such fractures. Depending on their thickness and lateral extent, basalt flow cores are likely to present caprocks in the NAIP, as seen in the Wallula injection site (McGrail et al., 2011). The mineralized and clogged flow crusts of the FIBG were seen to have low porosities (<5%) and low connected porosities, likely leading to low permeabilities. Unclogged vesicular basalts with porosities below the percolation threshold of ca. 29% are also likely to be low permeability. These crusts may also work as caprocks and contribute to the containment of CO_2. The volcaniclastic sediments have potentially high porosity. However, the permeability is low because of a high clay content. Previous studies of the reservoir properties of sedimentary interbeds in volcanic basalt sequences have shown that these properties are highly dependent on the depositional environment or sorting and later compaction and alteration (Ólavsdóttir et al., 2015; Reidel et al., 2002). There generally seems to be large variations in the reservoir properties of the volcaniclastic interbeds and they may display both reservoir and caprock properties. The large surface area of these rocks could lead to a high reactivity unless secondary mineralization is covering the grain surfaces. However, this study suggests red beds that are common in the FIBG and otherwise in the NAIP are likely to be low permeability, displaying caprock properties. These complex rock types require future appraisal to enable more robust predictions of their state in the sub-surface. Following the simulations presented by Wu et al. (2021), the vertical migration of gas-phase CO_2 from a permeable target into an overlying low-permeability zone (caprock) will likely also be inhibited by mineral precipitation, adding to the sealing effect of the caprock. A similar mechanism of "self-sealing" that has been proposed for fractured basaltic sills that form sealing units (Schmitt et al., 2022). It is also worth mentioning that in the Carbfix method CO_2 is dissolved in water before the injection, removing the need for a caprock as the gas is then no longer buoyant (Snæbjörnsdóttir et al., 2014).

4.3.3. Layer morphologies

McGrail et al. (2006) and Reidel et al. (2002) have previously used a threshold of minimum 15% porosity and 10 m thickness for potential

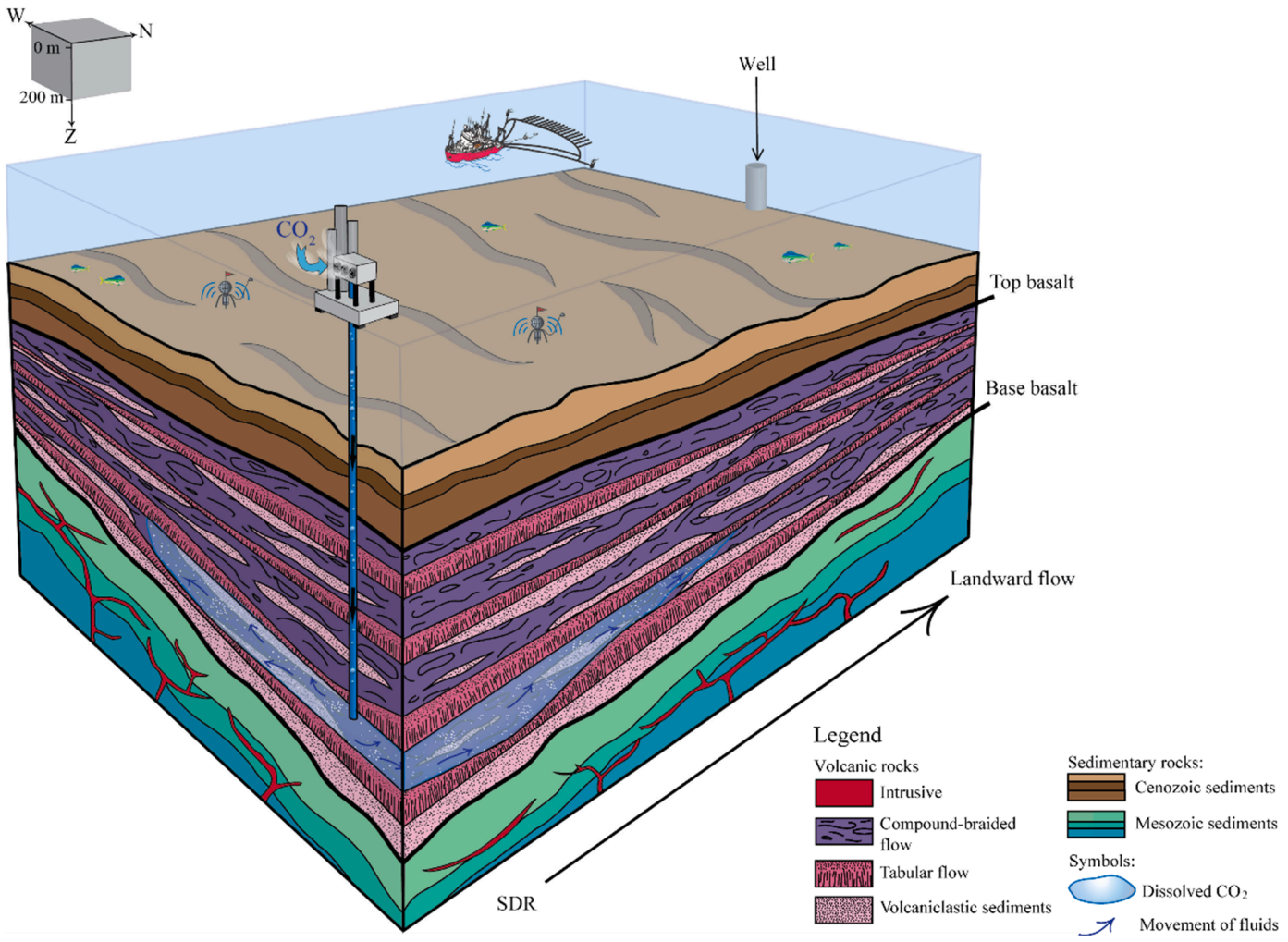

Fig. 11. Conceptual model of dissolved CO_2 being injected into an offshore volcanic reservoir of seaward-dipping reflectors (SDRs). The figure is based on volcanic sequences along the Vøring Margin High. The dissolved CO_2 is injected into basalt and will rapidly mineralize. Low permeability basalt layers (e.g., flow cores) may work as seals. Monitoring by seismic surveys or ocean-bottom seismometers may be needed in the initial phase but the CO_2 will rapidly be immobilized by in situ mineralization.

CO_2 reservoirs in basalt sequences, while Anthonsen et al. (2014) describe the preferred seal thickness for a CO_2-storage to be >50 m. The sedimentary interbeds were generally observed to be <2 m thick in the studied sequences. The volcaniclastic interbeds are, therefore, more likely to work as baffles than seals for CO_2 migration. The flow cores of simple flows, however, are seen to have a lateral extent on the km scale and a thickness up to ca. 25 m. The flow cores in these sequences may, therefore, work as seals if they are stacked in sealing units containing multiple low permeability layers, as seen at, e.g., the Wallula site (McGrail et al., 2011). The lateral extent of any such seal would have to be properly mapped out. The thickest flow crusts in the studied sequences were present as the flow tops of simple lava flows. The Flow 3 top is the only flow crust in the Glyvursnes-1 borehole that reaches a thickness of >10 m, and even though this crust is thought to be of low porosity and permeability, it shows that there is a potential for these layers to reach the required thickness threshold. In addition, faults and intrusions may affect fluid flow in the sequences and will need to be studied further in the future.

5. Applications for CO_2 storage

Significant secondary mineralization was observed in the pores of the upper FIBG on the Faroe Islands. The degree of alteration and secondary mineralization increases with the age of the rock and burial depth (Fisher, 1998). The FIBG is estimated to have been buried by between 700 and 2500 m of overburden that has been eroded (Andersen et al., 2002; Jørgensen, 2006). Precipitation of zeolites in the pores is expected to occur at depths exceeding ca. 1 km (Walton and Schiffman, 2003). In addition, higher confining pressure may decrease the permeability of basalts (Callow et al., 2018; Fisher, 1998), but this is also clearly dependent on volcanic facies (Millett et al., 2016). In the NAIP, the last erupted sequences of the province which were buried in the sub-surface before the extensive erosion that has stripped off the youngest and least altered intervals of the Faroe Islands Basalt Group may therefore contain the best reservoirs for CO_2 storage. The results presented herein support existing evidence that basaltic rocks provide good sources of divalent metal cations for potential carbonate precipitation (Gudbrandsson et al., 2011; Kelemen et al., 2019; Matter et al., 2016; Pogge von Strandmann et al., 2019), which can also occur in systems where seawater is the reservoir fluid (Voigt et al., 2021).

The fact that occurrences of flow crusts with little to no secondary mineralization in the pores are observed in the Faroe Islands basalt is encouraging for what may be found in potential offshore storage sites, more suitable for sequestration (Fig. 11). The Vøring and Møre margins off the Norwegian coast are examples of subaerial flood basalt sequences comparable to the outcrops on the Faroe Islands (Planke, 1994), and can be mapped with modern seismic data over a distance of more than 1000 km along the NE Atlantic margin from the Faroe Islands up to northern

Norway (Millett et al., 2020) The thickness of the lava sequence varies substantially from a few 10 s of m up to several kilometres along the margin and in many cases, geomorphological features on the top basalt surface in 3D seismic data reveal limited to no erosion (unlike the Faroe Islands, Planke et al., 2017). Evidence from the ODP 642E borehole on the Vøring Margin reveals subaerial basalt sequences containing unclogged vesicular lava flow crusts down to ca. 900 m depth (Planke, 1994), a feature also reported from provisional results from IODP Expedition 396 in the same area (Planke et al., 2022). These indications suggest that the good reservoir properties of volcanic sequences, prior to natural clogging and mineralization induced by greater initial burial depths and/or more pervasive hydrothermal alteration, may well be present in the offshore NAIP sequences. Storage in sub- or inter-basalt sediments may also form a possible additional option in the NAIP. At the Rosebank Field in the Faroe-Shetland Basin, hydrocarbon discoveries in inter- and sub-basalt sediments show that more conventional reservoirs are present within the volcanic sequences of the NAIP (Hardman et al., 2019; Millett et al., 2021; Schofield and Jolley, 2013). In offshore storage sites, overlying sedimentary caprocks in the post-volcanic sequences may present additional seals for CO_2 leakage scenarios and must be appraised as part of any site characterization in the future.

6. Conclusions

This study has reported the reservoir properties and reactivity of basalt lava flows and volcaniclastic rocks from subaerially erupted lava flow sequences of the Faroe Islands Basalt Group. The results were used to study potential reservoirs and seals for CO_2 storage in volcanic sequences of the North Atlantic Igneous Province.

- The best reservoir prospects seem to be the brecciated flow crusts of simple or tabular lava flows, that have not been clogged by secondary mineralization, as they display both high porosities, and high permeabilities, and may reach above required reservoir thicknesses. Additional reservoirs may be found in highly porous (above ca. 30%) vesicular basalts.
- The thin volcaniclastic red beds, though porous, are likely to work as bafflers for CO_2 migration due to their high clay content. While the best seals are likely present as flow cores of simple lava flows. Together with the volcaniclastic interbeds and clogged lava flow crust, they may create large, sealing packages.
- The results from the kinetic experiments show that the primary divalent cation released throughout the kinetic experiments was Ca^{2+}. This suggests that calcite (or aragonite in seawater systems) precipitation would be favoured in a CO_2 injection scenario (depending on the chemical conditions).
- The reactivity of the altered flow crusts and volcaniclastic sediments in the FIBG is dependent on the extent of alteration. Flow crusts are seen to have slower surface area normalized dissolution rates than the unaltered flow cores, although the presence of zeolite acts as a significant source of divalent cation promoting carbonate mineralization. The measured dissolution rates are indicating that the rocks would successfully mineralize CO_2.
- The results of this study show that there is a potential for finding porous, permeable, and reactive rocks, as well as impermeable seals ideal for CO_2 storage by in situ mineralization in offshore areas of the North Atlantic Igneous Province. The effect of faulting and fracturing, layer dimensions, and morphologies on CO_2 migration in volcanic sequences should be studied further.

Author statement

Marija P. Rosenqvist – Conceptualization, methodology, validation, formal analysis, investigation, writing (original draft and revising), visualization

Max W. J. Meakins – Conceptualization, methodology, validation, formal analysis, investigation, writing (original draft and revising), visualization

Sverre Planke – Conceptualization, validation, resources, writing (review and editing), supervision

John M. Millett - Conceptualization, validation, resources, writing (review and editing), supervision

Hans Jørgen Kjøll – Validation, writing (review and editing), supervision

Martin J. Voigt – Methodology, validation, resources, writing (review and editing)

Bjørn Jamtveit – Conceptualization, validation, resources, supervision, project administration, funding acquisition

Declaration of Competing Interest

The authors declare that they have no known competing financial interests or personal relationships that could have appeared to influence the work reported in this paper.

Data Availability

Data will be made available on request.

Acknowledgement

We acknowledge funding from the University of Oslo through the Department of Geosciences, the European Research Council (ERC) through the ERC Advanced Grant Disequilibrium metamorphism of stressed lithosphere (DIME) (ERC-2015-AdG_669972), the Cambridge Arctic Shelf Program (CASP) through the Andrew Whitham CASP Fieldwork Awards 2020, and the Faculty of Mathematics and Natural Sciences at the University of Oslo through the project *CO2Basalt*. S. Planke acknowledges support from the Norwegian Research Council through center of Excellence funding to CEED (project no. 223272). H. J. Kjøll acknowledges AkerBP for funding through the project *8040 Paleocene*. In addition, we thank the University of Iceland for covering the costs of the kinetic experiments. We would like to thank the Faroese Geological Survey (Jarðfeingi), Øyvind Hammer at the Museum of Natural History (Norway), Benjamin Bellwald at Volcanic Basin Energy Research (VBER), John Aiken from the Njord center, and Benoit Cordonnier from the European Synchrotron Radiation Facility (ESRF) in Grenoble, France, for their contributions to the project. Finally, we thank Sigurður Gíslason and the Carbfix team for providing laboratory facilities and assistance during part of this research.

Supplementary materials

Supplementary material associated with this article can be found, in the online version, at doi:10.1016/j.ijggc.2023.103838.

References

Abdelmalak, M.M., Faleide, J.I., Planke, S., Gernigon, L., Zastrozhnov, D., Shephard, G. E., Myklebust, R., 2017. The T-reflection and the deep crustal structure of the Vøring Margin, offshore mid-Norway. Tectonics 36 (11), 2497–2523.

Andersen, M.S., Sørensen, A.B., Boldreel, L.O., Nielsen, T., 2002. Cenozoic evolution of the Faroe Platform: comparing denudation and deposition. Geol. Soc. Lond. Spec. Publ. 196 (1), 291–311.

Anthonsen, K., Aagaard, P., Bergmo, P., Gislason, S., Lothe, A., Mortensen, G., Snæbjörnsdóttir, S., 2014. Characterisation and selection of the most prospective CO_2 storage sites in the Nordic region. Energy Procedia 63, 4884–4896.

Aradóttir, E., Sonnenthal, E., Björnsson, G., Jónsson, H, 2012. Multidimensional reactive transport modeling of CO2 mineral sequestration in basalts at the Hellisheidi geothermal field, Iceland. Int. J. Greenh. Gas Control 9, 24–40.

Avizo, (2016). Avizo 3D Software User's Guide. FEI. https://www.fei.com/software/avizo-user-guide/ (Accessed May 26, 2022).

Barnes, I., O'NEIL, J.R, 1969. The relationship between fluids in some fresh alpine-type ultramafics and possible modern serpentinization, western United States. Geol. Soc. Am. Bull. 80 (10), 1947–1960.

Barton, C., Moos, D., Blangy, J.-P., 1989. Analysis of full waveform acoustic logging data at ODP Site 642 - outer Vøring Plateau. Proc. Ocean Drill. Progr. Sci. Results 104, 953–964.

Benson, S., Cook, P., Anderson, J., Bachu, S., Nimir, H., Basu, B., Bradshaw, J., Deguchi, G., Gale, J., von Goerne, G., Heidug, W., Holloway, S., Kamal, R., Keith, D., Loyd, P., Rocha, P., Senior, B., Thomson, J., Torp, T., Wildenborg, T., Wilson, M., Zarlenga, F., Zhou, D., Celia, M., Gunter, B., King, J. E., Lindeberg, E., Lombardi, S., Oldenburg, C., Pruess, K., Rigg, A., Stevend, S., Wilson, E. S., Whittaker, S., 2005. Underground geological storage. In: Metz, B, Davidson, O, Coninck, H, Loos, M, L, M. (Eds.), IPCC Special Report on Carbon Dioxide Capture and Storage, 1st ed. Cambridge University Press, pp. 195–276.

Bernard, D., Nielsen, Ø., Salvo, L., Cloetens, P., 2005. Permeability assessment by 3D interdendritic flow simulations on microtomography mappings of Al–Cu alloys. Mater. Sci. Eng. A Struct. Mater. 392 (1–2), 112–120.

Broglia, C., Ellis, D, 1990. Effect of alteration, formation absorption, and standoff on the response of the thermal neutron porosity log in gabbros and basalts: examples from Deep Sea Drilling Project-Ocean Drilling Program Sites. J. Geophys. Res. 95 (B6), 9171–9188.

Broglia, C., Moos, D, 1988. In-situ structure and properties of 110-Ma crust from geophysical logs in DSDP Hole 418A. Proc. Ocean Drill. Progr. Sci. Results 102, 29–47.

Brunauer, S., Emmett, P.H., Teller, E., 1938. Adsorption of gases in multimolecular layers. J. Am. Chem. Soc. 60 (2), 309–319.

Burns, E.R., Snyder, D.T., Haynes, J.V., Waibel, M.S., 2012. Groundwater Status and Trends for the Columbia Plateau Regional Aquifer System, Washington, Oregon, and Idaho. U. S. Survey Scientific Investigations Report 2012-5261.

Callow, B., Falcon-Suarez, I., Ahmed, S., Matter, J., 2018. Assessing the carbon sequestration potential of basalt using X-ray micro-CT and rock mechanics. Int. J. Greenh. Gas Control 70, 146–156.

Chalmers, J.A., Waagstein, R., 2006. Scientific Results from the Deepened Lopra-1 Borehole, Faroe Islands. Geological Survey of Denmark and Greenland Bulletin, 156.

Clark, D.E., Oelkers, E.H., Gunnarsson, I., Sigfússon, B., Snæbjörnsdóttir, S.Ó., Aradottir, E.S., Gíslason, S.R., 2020. Carbfix2: CO_2 and H_2S mineralization during 3.5 years of continuous injection into basaltic rocks at more than 250° ca. Geochim. Cosmochim. Acta 279, 45–66.

Couves, C.R., 2015. Investigating the Petrophysical Properties of Volcanic Reservoir Analogues Through the Use of Micro-Focus X-Ray Computed Tomography. (Doctoral dissertation, University of Southampton).

Eidesgaard, Ó.R., 2021. Investigation and Applicability of Interpreted Well Log Data within the Faroe Islands Basalt Group. (Doctoral thesis, University of Copenhagen).

Ellis, D., Bell, B.R., Jolley, D.W., O'Callaghan, M, 2002. The stratigraphy, environment of eruption and age of the Faroes Lava Group, NE Atlantic Ocean. Geol. Soc. Lond. Spec. Publ. 197 (1), 253–269.

Ferreira, T., Radband, W., 2012. ImageJ User Guide. National Institutes of Health and the Laboratory for Optical and Computational Instrumentation. https://imagej.net/docs/guide/146.html#Noteworthy (Accessed May 22, 2022).

Fisher, A.T., 1998. Permeability within basaltic oceanic crust. Rev. Geophys. 36 (2), 143–182.

Gíslason, S.R., Oelkers, E.H., 2014. Carbon storage in basalt. Science 344 (6182), 373–374.

Gíslason, S.R., Sigurdardóttir, H., Aradóttir, E.S., Oelkers, E.H., 2018. A brief history of Carbfix: challenges and victories of the project's pilot phase. Energy Procedia 146, 103–114.

Goldberg, D.S., Takahashi, T., Slagle, A.L., 2008. Carbon dioxide sequestration in deep-sea basalt. Proc. Natl. Acad. Sci. 105 (29), 9920–9925.

Gudbrandsson, S., Wolff-Boenisch, D., Gislason, S.R., Oelkers, E.H., 2011. An experimental study of crystalline basalt dissolution from 2⩽ pH⩽ 11 and temperatures from 5 to 75 ca. Geochim. Cosmochim. Acta 75 (19), 5496–5509.

Gudbrandsson, S., Wolff-Boenisch, D., Gislason, S.R., Oelkers, E.H., 2014. Experimental determination of plagioclase dissolution rates as a function of its composition and pH at 22°C. Geochim. Cosmochim. Acta 139, 154–172.

Gunnarsson, I., Aradóttir, E.S., Oelkers, E.H., Clark, D.E., Arnarson, M.Þ., Sigfússon, B., Snæbjörnsdóttir, S.Ó., Matter, J.M., Stute, M., Júlíusson, B.M., 2018. The rapid and cost-effective capture and subsurface mineral storage of carbon and sulfur at the Carbfix2 site. Int. J. Greenh. Gas Control 79, 117–126.

Gysi, A., Stefánsson, A., 2008. Numerical modelling of CO2-water-basalt interaction. Mineral. Mag. 72 (1), 55–59.

Hardman, J., Schofield, N., Jolley, D., Hartley, A., Holford, S., Watson, D, 2019. Controls on the distribution of volcanism and intra-basaltic sediments in the Cambo–Rosebank region, West of Shetland. Pet. Geosci. 25 (1), 71–89.

IEA, 2021. Net Zero by 2050: A Roadmap for the Global Energy Sector. International Energy Agency (IEA).

IPCC, 2018. Summary for Policymakers. In: Masson-Delmotte, V.P.Zhai, Pörtner, H.-O., Roberts, D., Skea, J., Shukla, P.R., Pirani, A. (Eds.), et al., An IPCC Special Report on the Impacts of Global Warming of 1.5°C Above Pre Industrial Levels and Related Global Greenhouse Gas Emission Pathways, in the Context of Strengthening the Global Response to the Threat of Climate Change, Sustainable Development, and Efforts to Eradicate Poverty. World Meteorological Organization.

IPCC, 2021. Summary for Policymakers. In: Masson-Delmotte, V., Zhai, P., Pirani, A., Connors, S.L., ca. Péan, S.Berger, Caud, N., et al. (Eds.), Climate Change 2021: The Physical Science Basis. Contribution of Working Group I to the Sixth Assessment Report of the Intergovernmental Panel On Climate Change. Cambridge University Press, pp. 3–32.

Jolley, D.W., Passey, S.R., 2012. Lava-Sediment Interaction in a Near-Shore Environment: An Analogue for Offshore Exploration - Final Report (SINDRI Project: C46-38-01). The Sindri Group.

Japsen, P., Andersen, M.S., .Boldreel, L.O., .Waagstein, R., White, R.S., .and Worthington, M. (2006). Seismic and petrophysical properties of Faroes basalts (the SeiFaBa project Final Report). Geological Survey of Denmark and Greenland, Report 2006/29.

Jayne, R.S., Wu, H., Pollyea, R.M., 2019. Geologic CO_2 sequestration and permeability uncertainty in a highly heterogeneous reservoir. Int. J. Greenh. Gas Control 83, 128–139.

Jørgensen, O., 1984. Zeolite zones in the basaltic lavas of the Faeroe Islands: a quantitative description of the secondary minerals in the deep wells of Vestmanna-1 and Lopra-1. In: Berthelsen, O., Noe-Nygaard, A., Rasmussen, J. (Eds.), The Deep Drilling Project 1980-1981 in the Faeroe Islands, Supplementum IX, pp. 71–91.

Jørgensen, O., 2006. The regional distribution of zeolites in the basalts of the Faroe Islands and the significance of zeolites as palaeotemperature indicators. Geol. Surv. Den. Greenl. (GEUS) Bull. 9, 123–156.

Kelemen, P., Benson, S.M., Pilorgé, H., Psarras, P., Wilcox, J., 2019. An overview of the status and challenges of CO_2 storage in minerals and geological formations. Front. Clim. 1, 1–20.

Kelemen, P.B., Aines, R., Bennett, E., Benson, S.M., Carter, E., Coggon, J.A., De Obeso, J. C., Evans, O., Gadikota, G., Dipple, G.M., 2018. In situ carbon mineralization in ultramafic rocks: natural processes and possible engineered methods. Energy Procedia 146, 92–102.

Kelemen, P.B., Manning, ca.E., 2015. Reevaluating carbon fluxes in subduction zones, what goes down, mostly comes up. Proc. Natl. Acad. Sci. 112 (30), E3997–E4006.

Kelemen, P.B., Savage, H., Hirth, G., 2013. Reaction-driven cracking during mineral hydration, carbonation and oxidation. In: Poromechanics V: Proceedings of the Fifth Biot Conference on Poromechanics, pp. 823–826.

Kesraoui-Ouki, S., Cheeseman, C., Perry, R, 1993. Effects of conditioning and treatment of chabazite and clinoptilolite prior to lead and cadmium removal. Environ. Sci. Technol. 27 (6), 1108–1116.

Kirkpatrick, S., 1973. Percolation and conduction. Rev. Mod. Phys. 45 (4), 574–588.

Lundegard, P.D., 1992. Sandstone porosity loss; a" big picture" view of the importance of compaction. J. Sediment. Res. 62 (2), 250–260.

Matter, J.M., Broecker, W., Gislason, S., Gunnlaugsson, E., Oelkers, E., Stute, M., Sigurdardóttir, H., Stefansson, A., Alfreðsson, H., Aradóttir, E., 2011. The Carbfix Pilot Project—storing carbon dioxide in basalt. Energy Procedia 4, 5579–5585.

Matter, J.M., Broecker, W., Stute, M., Gislason, S., Oelkers, E., Stefánsson, A., Wolff-Boenisch, D., Gunnlaugsson, E., Axelsson, G., Björnsson, G., 2009. Permanent carbon dioxide storage into basalt: the Carbfix pilot project, Iceland. Energy Procedia 1 (1), 3641–3646.

Matter, J.M., Stute, M., Snæbjörnsdottir, S.Ó., Oelkers, E.H., Gislason, S.R., Aradottir, E. S., Sigfusson, B., Gunnarsson, I., Sigurdardottir, H., Gunnlaugsson, E., 2016. Rapid carbon mineralization for permanent disposal of anthropogenic carbon dioxide emissions. Science 352 (6291), 1312–1314.

Mavko, G., Nur, A., 1997. The effect of a percolation threshold in the Kozeny-Carman relation. Geophysics 62 (5), 1480–1482.

McGrail, B., Spane, F., Sullivan, E., Bacon, D., Hund, G., 2011. The Wallula basalt sequestration pilot project. Energy Procedia 4, 5653–5660.

McGrail, B.P., Schaef, H.T., Ho, A.M., Chien, Y.J., Dooley, J.J., Davidson, ca.L., 2006. Potential for carbon dioxide sequestration in flood basalts. J. Geophys. Res. 111 (B12), 1–13.

McGrail, B.P., Schaef, H.T., Spane, F.A., Horner, J.A., Owen, A.T., Cliff, J.B., Qafoku, O., Thompson, ca.J., Sullivan, E.ca, 2017. Wallula Basalt pilot demonstration project: post-injection results and conclusions. Energy Procedia 114, 5783–5790.

Millett, J., Hole, M., Jolley, D., Passey, S., 2017. Geochemical stratigraphy and correlation within large igneous provinces: the final preserved stages of the Faroe Islands Basalt Group. Lithos 286, 1–15.

Millett, J., Hole, M., Jolley, D., Passey, S.R., Rossetti, L., 2020. Transient mantle cooling linked to regional volcanic shut-down and early rifting in the North Atlantic Igneous Province. Bull. Volcanol. 82 (8), 1–27.

Millett, J.M., Jerram, D.A., Manton, B., Planke, S., Ablard, P., Wallis, D., Hole, M.J., Brandsen, H., Jolley, D.W., Dennehy, C., 2021. The Rosebank Field, NE Atlantic: volcanic characterization of an inter-lava hydrocarbon discovery. Basin Res 33, 2883–2913.

Millett, J., Wilkins, A., Campbell, E., Hole, M., Taylor, R., Healy, D., Jerram, D., Jolley, D., Planke, S., Archer, S., 2016. The geology of offshore drilling through basalt sequences: understanding operational complications to improve efficiency. Mar. Pet. Geol. 77, 1177–1192.

Neuhoff, P.S., Fridriksson, T., Arnorsson, S., Bird, D.K., 1999. Porosity evolution and mineral paragenesis during low-grade metamorphism of basaltic lavas at Teigarhorn, eastern Iceland. Am. J. Sci. 299 (6), 467–501.

Noe-Nygaard, A., Rasmussen, J., 1968. Petrology of a 3,000 meter sequence of basaltic lavas in the Faeroe Islands. Lithos 1 (3), 286–304.

Ólavsdóttir, J., Andersen, M.S., Boldreel, L.O., 2015. Reservoir quality of intrabasalt volcaniclastic units onshore Faroe Islands, North Atlantic Igneous Province, northeast Atlantic. Am. Assoc. Pet. Geol. Bull. 99 (3), 467–497.

Passey, S.R., Bell, B.R., 2007. Morphologies and emplacement mechanisms of the lava flows of the Faroe Islands Basalt Group, Faroe Islands, NE Atlantic Ocean. Bull. Volcanol. 70 (2), 139–156.

Passey, S.R., Jolley, D.W., 2009. A revised lithostratigraphic nomenclature for the Palaeogene Faroe Islands Basalt Group, NE Atlantic Ocean. Earth Environ. Sci. Trans. R Soc. Edinb. 99 (3–4), 127–158.

Planke, S., 1994. Geophysical response of flood basalts from analysis of wire line logs: ocean Drilling Program Site 642, Vøring volcanic margin. J. Geophys. Res. 99 (B5), 9279–9296.
Planke, S., Bellwald, B., Millett, J., Planke, E.E., Zastrozhnov, D., Carlevaris, P., Jamtveit, B., Rosenqvist, M., Jerram, D., Schmid, D.W., Berndt, C., Kjølhamar, B., Myklebust, R., 2020. Permanent carbon sequestration potential in offshore basalt sequences on the NW European continental margins. In: European Association of Geoscientists and Engineers, Conference Proceedings, 82nd EAGE Annual Conference and Exhibition, Amsterdam, Netherlands.
Planke, S., Berndt, C., Zarikian, Alvarez, the Expedition 396 Scientists, 2022. Expedition 396 Preliminary Report: Mid-Norwegian Margin Magmatism and Paleoclimate Implications. International Ocean Discovery Program, 2372–9562.
Planke, S., Millett, J.M., Maharjan, D., Jerram, D.A., Abdelmalak, M.M., Groth, A., Hoffmann, J., Berndt, C., Myklebust, R., 2017. Igneous seismic geomorphology of buried lava fields and coastal escarpments on the Vøring volcanic rifted margin. Interpretation 5 (3), SK161–SK177.
Pogge von Strandmann, P.A., Burton, K.W., Snæbjörnsdóttir, S.O., Sigfússon, B., Aradóttir, E.S., Gunnarsson, I., Alfredsson, H.A., Mesfin, K.G., Oelkers, E.H., Gislason, S.R., 2019. Rapid CO_2 mineralisation into calcite at the Carbfix storage site quantified using calcium isotopes. Nat. Commun. 10 (1), 1–7.
Pollyea, R.M., Rimstidt, J.D., 2017. Rate equations for modeling carbon dioxide sequestration in basalt. Appl. Geochem. 81, 53–62.
Rasmussen, J., Noe-Nygaard, A., 1970. Geology of the Faeroe Islands (Pre-Quaternary). Geol. Surv. Den. Cph. 1, 1–25.
Reed, S.J.B., 2005. Electron Microprobe Analysis and Scanning Electron Microscopy in Geology. Cambridge university press, pp. 1–206.
Reidel, S.P., Spane, F.A., Johnson, V.G, 2002. Natural Gas Storage in Basalt Aquifers of the Columbia Basin, Pacific Northwest USA: A Guide to Site Characterization. Rep. PNNL-13962. Pac. Northwest Natl. Lab.
Rintoul, M.D., Torquato, S., 1997. Reconstruction of the structure of dispersions. J. Colloid Interface Sci. 186 (2), 467–476.
Røyne, A., Jamtveit, B., 2015. Pore scale controls on reaction driven fracturing. Rev. Mineral. Geochem. 80, 26–44.
Saunders, A., Fitton, J., Kerr, A.C., Norry, M., Kent, R., 1997. The North Atlantic Igneous Province. Geophys. Monogr. Am. Geophys. Union 100, 45–94.
Schaef, H.T., McGrail, B.P., 2009. Dissolution of Columbia River Basalt under mildly acidic conditions as a function of temperature: experimental results relevant to the geological sequestration of carbon dioxide. Appl. Geochem. 24 (5), 980–987.
Schlumberger, 1987. Log interpretation : Principles/Applications. Schlumberger Educational Services.
Schofield, N., Jolley, D.W., 2013. Development of intra-basaltic lava-field drainage systems within the Faroe–Shetland Basin. Pet. Geosci. 19 (3), 273–288.
Schwertmann, U., 1991. Solubility and dissolution of iron oxides. Plant Soil 130 (1), 1–25.
Seifritz, W., 1990. CO_2 disposal by means of silicates. Nature 345 (6275), 486. -486.
Self, S., Thordarson, T., Keszthelyi, L., Walker, G., Hon, K., Murphy, M., Long, P., Finnemore, S., 1996. A new model for the emplacement of Columbia River basalts as large, inflated pahoehoe lava flow fields. Geophys. Res. Lett. 23 (19), 2689–2692.
Selley, R., 1976. An Introduction to Sedimentology.Academic. Press Inc, pp. 1–417.
Sigfusson, B., Gislason, S.R., Matter, J.M., Stute, M., Gunnlaugsson, E., Gunnarsson, I., Aradottir, E.S., Sigurdardottir, H., Mesfin, K., Alfredsson, H.A, Wolff-Boenisch, D., Arnarsson, M.T., Oelkers, E.H., 2015. Solving the carbon-dioxide buoyancy challenge: the design and field testing of a dissolved CO_2 injection system. Int. J. Greenh. Gas Control 37, 213–219.
Schmitt, R.R., Andrews, G.D., Moore, J., Paronish, T., Workman, S., Gumowski, L.M., Brown, S.R., Crandall, D., Neubaum, J., 2022. Self-sealing mafic sills for carbon and hydrogen storage. Geol. Soc. Lond. Spec. Publ. 528 (1), SP528–S2022.
Snæbjörnsdóttir, S.Ó., Gislason, S.R., Galeczka, I.M., Oelkers, E.H., 2018. Reaction path modelling of in-situ mineralisation of CO2 at the Carbfix site at Hellisheidi, SW-Iceland. Geochim. Cosmochim. Acta 220, 348–366.
Snæbjörnsdóttir, S.Ó., Sigfússon, B., Marieni, C., Goldberg, D., Gislason, S.R., Oelkers, E. H., 2020. Carbon dioxide storage through mineral carbonation. Nat. Rev. Earth Environ. 1 (2), 90–102.
Snæbjörnsdóttir, S.Ó., Wiese, F., Fridriksson, T., Ármansson, H., Einarsson, G.M., Gislason, S.R., 2014. CO_2 storage potential of basaltic rocks in Iceland and the oceanic ridges. Energy Procedia 63, 4585–4600.
Stockmann, G.J., Wolff-Boenisch, D., Gislason, S.R., Oelkers, E.H., 2011. Do carbonate precipitates affect dissolution kinetics? 1: basaltic glass. Chem. Geol. 284 (3–4), 306–316.
Sun, S.-S., McDonough, W.F., 1989. Chemical and isotopic systematics of oceanic basalts: implications for mantle composition and processes. Geol. Soc. Lond. Spec. Publ. 42 (1), 313–345.
Saar, M.O., Manga, M., 1999. Permeability-porosity relationship in vesicular basalts. Geophys. Res. Lett. 26 (1), 111–114.
Tutolo, B.M., Awolayo, A., Brown, ca, 2021. Alkalinity generation constraints on basalt carbonation for carbon dioxide removal at the Gigaton-per-Year scale. Environ. Sci. Technol. 55 (17), 11906–11915.
UN. (2015). The Paris agreement. Report of the Conference of the Parties on its twenty-first session, held in Paris from 30 November to 13 December 2015.
Van Pham, T.H., Aagaard, P., Hellevang, H., 2012. On the potential for CO_2 mineral storage in continental flood basalts–PHREEQC batch- and 1D diffusion–reaction simulations. Geochem. Trans. 13 (1), 1–12.
Voigt, M., Marieni, C., Baldermann, A., Galeczka, I.M., Wolff-Boenisch, D., Oelkers, E.H., Gislason, S.R., 2021. An experimental study of basalt–seawater–CO_2 interaction at 130° ca. Geochim. Cosmochim. Acta 308, 21–41.
Waagstein, R., 2002a. *Composite well log: Glyvursnes-1, Faroe Islands* [Data set]. Geological Survey of Denmark and Greenland.
Waagstein, R., Guise, P., Rex, D., 2002b. K/Ar and 39Ar/40Ar whole-rock dating of zeolite facies metamorphosed flood basalts: the upper Paleocene basalts of the Faroe Islands, NE Atlantic. Special Publications 197 (1). Geological Society, London, pp. 219–252.
Walker, G., 1972. Compound and simple lava flows and flood basalts. Bull. Volcanol. 35 (3), 579–590.
Walker, R.J., Holdsworth, R., Imber, J., Ellis, D, 2011a. Onshore evidence for progressive changes in rifting directions during continental break-up in the NE Atlantic. J. Geol. Soc. Lond. 168 (1), 27–48.
Walton, A.W., Schiffman, P., 2003. Alteration of hyaloclastites in the HSDP 2 Phase 1 Drill Core 1. Description and paragenesis. Geochem. Geophys. Geosyst. 4 (5), 1–31.
Wolff-Boenisch, D., Galeczka, I., 2018. Flow-through reactor experiments on basalt-(sea) water-CO2 reactions at 90°C and neutral pH. What happens to the basalt pore space under post-injection conditions? Int. J. Greenh. Gas Control 68, 176–190.
Wolff-Boenisch, D., 2011. On the buffer capacity of CO2-charged seawater used for carbonation and subsequent mineral sequestration. Energy Procedia 4, 3738–3745.
Wu, H., Jayne, R.S., Bodnar, R.J., Pollyea, R.M., 2021. Simulation of CO2 mineral trapping and permeability alteration in fractured basalt: implications for geologic carbon sequestration in mafic reservoirs. Int. J. Greenh. Gas Control 109, 103383.
Waagstein, R., 1988. Structure, composition and age of the Faeroe basalt plateau. Geol. Soc. Lond. Spec. Publ. 39 (1), 225–238.
Waagstein, R., 1998. A Geological Field Guide to the Palaeogene Flood Basalts of Suðuroy, Faroe Islands. Geological Survey of Denmark and Greenland.
Zakharova, N.V., Goldberg, D.S., Sullivan, E.C., Herron, M.M., Grau, J.A., 2012. Petrophysical and geochemical properties of Columbia River flood basalt: implications for carbon sequestration. Geochem. Geophys. Geosyst. 13 (11), 1–22.
Zhu, W., Fusseis, F., Lisabeth, H., Xing, T., Xiao, X., De Andrade, V., Karato, S.i., 2016. Experimental evidence of reaction-induced fracturing during olivine carbonation. Geophys. Res. Lett. 43 (18), 9535–9543.